https://doi.org/10.5194/egusphere-2026-3160
Preprint. Discussion started: 23 June 2026

Global budgets of atmospheric primary and secondary organic aerosols constrained by full-volatility-range organic emissions

Ruqian Miao[1], Ruochong Xu[2], Shan Huang[3], Sihan Xiao[1], Hao Wang[1], Yan Zheng[1, a], Siyi Liu[1], Jingxian Li[4], Guannan Geng[4], Manish Shrivastava[5], Xu Dao[6], Claire Granier[7,12], Guy Brasseur[8], Vlassis A. Karydis[9], Alexandra P. Tsimpidi[9], Jianhui Jiang[10], Kaspar R. Daellenbach[11], Imad El Haddad[11,1], André S. H. Prévôt[11], Qi Chen[1, *]

[1]State Key Laboratory of Regional Environment and Sustainability, IJRC, College of Environmental Sciences and Engineering, Peking University, Beijing, China
[2]Department of Earth System Science, Ministry of Education Key Laboratory for Earth System Modeling, Institute for Global Change Studies, Tsinghua University, Beijing, China
[3]Institute for Environmental and Climate Research, Jinan University, Guangzhou, China
[4]State Key Joint Laboratory of Environment Simulation and Pollution Control, School of Environment, Tsinghua University, Beijing, China
[5]Pacific Northwest National Laboratory, Richland, Washington, USA
[6]China National Environmental Monitoring Centre, Beijing, China
[7]Laboratoire d'Aérologie, CNRS and University of Toulouse, Toulouse, France
[8]Environmental Modelling Group, Max Planck Institute for Meteorology, Hamburg, Germany
[9]Institute of Energy and Climate Research: Troposphere (ICE-3), Forschungszentrum Jülich GmbH, Jülich, Germany
[10]State Key Laboratory of Estuarine and Coastal Research, School of Ecological and Environmental Sciences, East China Normal University, Shanghai, China
[11]Laboratory of Atmospheric Chemistry, Paul Scherrer Institute, Villigen, Switzerland
[12]Chemical Sciences Laboratory, NOAA/CIRES, University of Colorado, Boulder, Colorado, USA
[a]now at: Division of Environment and Sustainability, The Hong Kong University of Science and Technology, Hong Kong, China

[*]*Correspondence to*: Qi Chen (qichenpku@pku.edu.cn)

Abstract. Organic aerosol (OA) constitutes a major fraction of tropospheric submicron particulate matter, with primary (POA) and secondary (SOA) components exhibiting different physicochemical properties and health impacts. The POA and SOA budgets are however highly uncertain, and the results from different model studies are confusing because of more or less consideration of the volatility distributions of organic precursor emissions and inconsistent attributions of model tracers in model-observation comparisons. Here we develop an OA simulation framework in GEOS-Chem that resolves the full volatility spectrum of organic precursor emissions from anthropogenic sources and open biomass burning. The model reasonably reproduces the observed OC, POA, and SOA concentrations from comprehensive surface, shipborne, and airborne datasets, providing a consistent global validation. The model simulations suggest greater POA (0.5 Tg) and SOA burdens (2.0 Tg) and potentially stronger and more widespread impacts of the OA components on air quality, health, and radiation than previous estimates, led by both of the emission updates and the revised OA scheme. The simulated global SOA production is about 106 Tg in 2018, 46% of which is contributed by open biomass burning. The results demonstrate distinct regional variations in the dominant source types and population exposure distributions of POA and SOA,

https://doi.org/10.5194/egusphere-2026-3160
Preprint. Discussion started: 23 June 2026

highlighting the needs for SOA mitigation, multi-sector control measures, and clean energy replacements for long-term health-oriented air quality improvements globally. The model results are sensitive to the emissions and wet-deposition parameterization, calling for more measurement constraints on local emission factors and the deposition fluxes of OA and its components.

1 Introduction

Organic aerosol (OA) constitutes a major fraction of tropospheric submicron particulate matter, with important implications for air pollution, climate, and human health (Jimenez et al., 2009; Heald et al., 2014; Shiraiwa et al., 2017; Shrivastava et al., 2017). OA comprises primary organic aerosol (POA), emitted directly or formed immediately by gas-particle partitioning of semi-volatile organic gases, and secondary organic aerosol (SOA), formed through atmospheric multiphase chemical oxidation of organic precursors. These components differ fundamentally in physicochemical properties and climate and human health impacts. SOA is generally more hygroscopic and thus more effective at forming cloud condensation nuclei (Thalman et al., 2017). Differences in chromophore composition lead to distinct optical properties of POA and SOA (Lin et al., 2014; Li et al., 2025). Moreover, both POA and SOA contribute to aerosol oxidative potential (Verma et al., 2015; Daellenbach et al., 2020), yet epidemiological evidence in the United States suggests a stronger association of long-term SOA exposure with cardiopulmonary mortality than POA (Pye et al., 2021; Pond et al., 2022). These contrasts underscore the need for quantitative constraints on POA and SOA at the global scale.

Despite decades of development, chemical transport models (CTMs) still struggle to represent OA consistently (Hallquist et al., 2009; Tsigaridis et al., 2014; Hodzic et al., 2016; Riipinen et al., 2026). A central challenge lies in the wide volatility spectrum of organic precursors, spanning semivolatile and low-volatility organic compounds (S/LVOCs; $C^* < 300$ μg/m^3), intermediate-volatility organic compounds (IVOCs; 300 μg/m^3 < C^* < 3×10^6 μg/m^3), and volatile organic compounds (VOCs) ($C^* > 3\times10^6$ μg/m^3) (Donahue et al., 2012). While VOC emissions are relatively well constrained, emissions of S/LVOCs and IVOCs remain highly uncertain. Most models infer S/LVOCs from bulk organic carbon (OC) emissions without resolving volatility distributions, leading to systematic biases (Pye and Seinfeld, 2010; Jathar et al., 2011; Shrivastava et al., 2015; Hodzic et al., 2016). Assuming nonvolatile POA in CTM can overestimate the POA concentrations by over 100% in outflow and remote regions (Jo et al., 2013; Murphy et al., 2017; Brewer et al., 2023). By contrast, CTM could reproduce the large fractional contributions of oxidized OA observed in the atmosphere only if some of the S/LVOCs in the model were allowed to evaporate and subsequently oxidize in the atmosphere (Shrivastava et al., 2008). Overly volatile assumptions however underestimate urban POA by over 50% (Woody et al., 2016; Jiang et al., 2019; Miao et al., 2021). Uncertainties are even larger for IVOCs, whose emissions are typically derived from proxies such as POA, non-methane VOCs (NMVOCs), and speciated IVOCs (i.e., naphthalene) using empirical scaling (Shrivastava et al., 2008; Hodzic et al., 2016; Pye and Seinfeld, 2010). Global emission estimates of IVOCs span more than an order of magnitude (16.2 Tg yr^{-1} to 234 Tg yr^{-1}) (Jathar et al., 2011; Hodzic et al., 2016; Pye and Seinfeld, 2010; Miao et al., 2021), with substantial discrepancies in source

https://doi.org/10.5194/egusphere-2026-3160
Preprint. Discussion started: 23 June 2026

attribution, seasonality, and spatial distributions. For example, POA-based estimates show greater emissions from residential combustion and stronger seasonal variation than NMVOC-based estimates (Miao et al., 2021; Yang et al., 2025). These uncertainties propagate directly into SOA formation, where yields vary strongly with volatility and molecular structure, ranging from <0.1 to >0.4 for IVOCs (Lu et al., 2020).

Recent advances now enable a more explicit treatment of this complexity. New bottom-up inventories quantify emissions across the full volatility range—from VOCs to S/LVOCs—using measurements from advanced mass spectrometry (Chang et al., 2022; Pye et al., 2023; Huang et al., 2023; Xu et al., 2026). The newly-developed MEIC-global-FVOC inventory incorporates sector and region-specific emission factors and suggests 28-41% higher global anthropogenic emissions of full-volatility range organic compounds (FVOCs) than previous estimates (Xu et al., 2026). These volatility-resolved emissions enable more mechanistic representations of SOA formation. For example, model studies incorporating volatility-binned IVOCs with bin-specific SOA yields report substantially reduced urban-rural differences with enhanced SOA concentrations (Lu et al., 2020; Miao et al., 2021; Manavi and Pandis, 2024; Scholz et al., 2025), suggesting greater and more widespread health impacts of OA than previously recognized. However, evaluations of such frameworks remain limited, particularly at the global scale, and constraints on POA–SOA partitioning are still sparse.

Here we develop a global OA simulation framework in the GEOS-Chem chemical transport model that resolves emissions across the full volatility spectrum. We evaluate model performance against a comprehensive observation dataset that includes surface, shipborne, and airborne measurements, and further assess POA and SOA against aerosol mass spectrometer source apportionment. This framework enables a quantitative reassessment of the global distribution and budget of POA and SOA, providing new constraints on their sources and variability.

2 Methods

2.1 Model configurations

We use the GEOS-Chem (version 14.3.0, DOI: 10.5281/zenodo.10640536) to simulate OA. Global simulations are run at 2° × 2.5° horizontal resolution with a vertical resolution of 47 layers from surface to 0.01 hPa. Nested-grid simulations are conducted over North America, Europe, Asia, and the Atlantic Ocean at a horizontal resolution of 0.5° × 0.625°, with boundary conditions from the global simulations. All simulations are driven by meteorological data from the MERRA2 reanalysis with a one-month spin-up. The base year for our simulations is 2018.

The model includes ozone-NO_x-hydrocarbon-aerosol-halogen chemistry for the troposphere (Bey et al., 2001). The ISORROPIA-II thermodynamic module is applied to simulate sulfate-nitrate-ammonium aerosols (Fountoukis and Nenes, 2007; Pye et al., 2009). Dry deposition is calculated by a standard resistance-in-series model (Wang et al., 1998; Zhang et al., 2001). Wet deposition includes wet convective updrafts and large-scale precipitation (Liu et al., 2001). The scavenging efficiencies of different types of aerosols in wet deposition depend on their hydrophilicity without considering the effect of

https://doi.org/10.5194/egusphere-2026-3160
Preprint. Discussion started: 23 June 2026

aging processes. For example, the scavenging efficiencies of POA and SOA are set to be 50% and 80%, respectively (Chung and Seinfeld, 2002; Miao et al., 2021).

For pollutants other than organic precursors, anthropogenic emissions in China and the rest of the world are provided by the Multi-resolution Emission Inventory model for Climate and air pollution research (MEIC) and the Community Emissions Data System (CEDS), respectively (Geng et al., 2024; Hoesly et al., 2018). Open biomass burning emissions are provided by the Fire Inventory from the National Center for Atmospheric Research (NCAR) version 2.5 (FINNv2.5) (Wiedinmyer et al., 2023). Soil NO_x emissions are calculated by the Berkeley-Dalhousie Soil NO_x Parameterization (BDSNP) (Hudman et al., 2012). Biogenic emissions are calculated by the Model of Emissions of Gases and Aerosols from Nature (MEGAN v2.1) (Guenther et al., 2012).

2.2 Full-volatility-range OA scheme

The standard GEOS-Chem model includes two OA schemes named as "simple OA" and "complex OA". The simple OA scheme treats POA as non-volatile and applies fixed yields to estimate SOA, whereas the complex OA scheme treats POA as semivolatile with more sophisticated parameterization and SOA yields (Pai et al., 2020). The complex OA scheme is firstly described by Pye and Seinfeld (2010), which considers SOA from VOCs, IVOCs, and S/LVOCs. In this scheme, all IVOC emissions are allocated to one lumped species with a SOA yield referring to naphthalene. IVOC emissions are estimated as 66 times of naphthalene emissions, which are approximated from benzene by the approach suggested by Pye and Seinfeld (2010). For S/LVOCs, their emissions are 1.27 and 1 times of the OC emissions for anthropogenic sources and open biomass burning, provided by CEDS and FINNv2.5, respectively, following an update suggested by Pai et al. (2020). The 49% and 51% of the S/LVOC emissions are allocated to the two lumped species with C^* of 1646 and 20 μg m^{-3}, respectively (Shrivastava et al., 2006). The complex OA scheme also has an option to treat POA as non-volatile, which is no longer recommended because of the large SOA underestimation (Schroder et al., 2018).

The full-volatility-range OA scheme is built based on the complex OA scheme in GEOS-Chem (Pye et al., 2010; Pai et al., 2020). The graphical overviews of these two schemes are shown in Figure S1, and their OA tracers are listed in Table S1 in the Supplement. First, a volatility-basis-set (VBS) approach with updated NO_x-dependent SOA yields is used to simulate the SOA production from the oxidation of isoprene, terpenes, and aromatics. The updates in SOA yields and vapor wall-loss corrections aim to better represent the low-loading gas-particle partitioning (Zhang et al., 2014; Chen et al., 2024). Vapor wall-loss correction factors of 1.2, 1.9, and 2.2 are used for the oxidation of aromatics under high-NO_x conditions, the oxidation of aromatics under low-NO_x conditions, and the high-NO_x pathway of isoprene SOA formation, respectively. The heterogeneous uptake of isoprene epoxydiols (IEPOX) on aerosols is included, which applies parameterizations on aerosol acidity and nucleophile concentration-sensitive reactive uptake coefficients (Marais et al., 2016). To avoid double counting in low-NO_x conditions, the traditional low-NO_x pathway for isoprene SOA formation is turned off (Pai et al., 2020).

https://doi.org/10.5194/egusphere-2026-3160
Preprint. Discussion started: 23 June 2026

Additionally, the heterogeneous reactions of glyoxal and methylglyoxal on aerosols are included, for which fixed reactive uptake coefficients are applied (Marais et al., 2016).

Unlike the default scheme for which tracers only represent limited volatility bins, the full-volatility-range OA scheme deals with continuously binned OA precursors and their oxidation processes (Figure 1). IVOCs are represented by four lumped species that have decadal saturation concentrations (C^*) ranging from 10^3 to 10^6 μg m^{-3}, and the SOA production from the oxidation of IVOCs is simulated by the VBS approach. The SOA yields of IVOC species are listed in Table S2 in the Supplement. Under high-NO_x conditions, the SOA yields derived from the photooxidation of *n*-alkanes are applied to the lumped IVOC species to represent the increasing SOA yields with the decreasing volatility of IVOC species (Presto et al., 2010; Zhao et al., 2014). We apply the same SOA yields for the IVOC species with C^* of 10^3 and 10^4 μg m^{-3} due to the lack of experiments for IVOC species with carbon numbers over 17 in their formulae. Under low-NO_x conditions, the IVOC SOA is treated as nonvolatile mass with a constant SOA yield of 73% (Chan et al., 2009; Pye and Seinfeld, 2010). In addition, the IVOC SOA yields are corrected for vapor wall loss with a correction factor of 1.2 for both low- and high-NO_x pathways (Zhang et al., 2014). For S/IVOCs, the gas phase has four lumped species that have decadal C^* ranging from 10^{-1} to 10^2 μg m^{-3}, whereas the particle-phase portion is represented by five lumped species with decadal C^* of 10^{-2} to 10^2 μg m^{-3}. Then the gas-phase S/LVOCs undergo photooxidation with a rate constant of 2×10^{-11} cm^3 $molec^{-1}$ s^{-1} in the scheme to produce oxidation products with 100 times lower C^* than their precursors (Pye and Seinfeld, 2010). These low-volatility products follow gas-particle partitioning to form SOA. After emission and dilution, the S/LVOCs that remain in or recondense into the particle phase without undergoing any chemical processing are classified as POA.

Anthropogenic emissions of the 9-bin lumped organic species are provided by the newly-developed MEIC-global-FVOC inventory (Xu et al., submitted). MEIC-global-FVOC estimates the emissions of organic species by a bottom-up approach under the framework of MEIC based on activity rates, technology distributions, unabated emission factors for different regions, and available control technologies. The emission factors for volatility-binned S/LVOCs and IVOCs from C^* of 10^{-2} to 10^6 μg m^{-3} are harmonized from recent emission characterization experiments for various sources by advanced measurement techniques, such as two-dimensional gas chromatography-time-of-flight mass spectrometry (GC × GC−TOF−MS), thermal desorption-gas chromatography/mass spectrometry (TD-GC-MS), proton-transfer-reaction time-of-flight mass spectrometer (PTR-ToF-MS). Major source sectors in this inventory include coal combustion, oil combustion, biomass combustion, fugitive and industrial processes, and volatile chemical products (VCPs) for industrial and domestic uses. The emission factors of S/LVOCs for biomass combustion of wood and crop for developing regions such as China, India, and African countries are further constrained by local emission factors of OC to reduce the biases in mass closure of S/LVOCs in analytical detection and the regional differences in stove types and combustion conditions. Moreover, empirical scaling factors of 4 and 6 are applied to the residential biofuel combustion-related S/LVOC emissions in Western and Eastern Europe, respectively. Without these scaling factors, the simulated concentrations of biomass burning-related OA (BBOA) are much lower than the observation-derived BBOA concentrations (Figure S2 in the Supplement).

https://doi.org/10.5194/egusphere-2026-3160
Preprint. Discussion started: 23 June 2026

Waste treatments and open biomass burning are not represented by MEIC-global-FVOC. We follow our previous work to apply emission ratios to NMVOC and OC to derive the total amounts of IVOC and S/LVOC emissions of these sources, respectively, and then distribute the emissions to volatility bins based on assumed volatility distributions (Chen et al., 2024). The emissions from waste treatments that are proportional to the waste-related NMVOC and OC emissions from CEDS are added as additional anthropogenic emissions. This source is important in populated urban areas in developing regions (e.g., Africa and India), where incineration of municipal solid waste occurs without any pollution control (Sharma et al., 2019; McDuffie et al., 2020). The empirical emission ratios for waste treatments are listed in Table S3 in the Supplement. The total anthropogenic IVOC and S/LVOC emissions in 2018 are 37.4 Tg and 25.4 Tg, respectively (spatial distributions shown in Figure S3a in the Supplement). For open biomass burning, the emissions of IVOC and S/LVOC are derived from the NMVOC and OC emissions from FINNv2.5 with empirical scalars listed in Table S3 (Chen et al., 2024; Wiedinmyer et al., 2023). The total IVOC and S/LVOC emissions from open biomass burning are 36.7 Tg and 38.5 Tg in 2018, respectively. The spatial distributions of IVOC and S/LVOC emissions from open biomass burning are shown in Figure S3b in the Supplement. In addition, biogenic emissions for isoprene and terpenes are calculated by MEGAN v2.1, and the biomass burning emissions for VOC precursors such as isoprene, terpenes, and aromatics are provided by FINNv2.5.

Configurations of the model runs are listed in Table S4 in the Supplement. Simulation runs with the full-volatility-range OA scheme and the FVOC emissions are named as “Base”, while the default complex OA scheme-based simulation runs are named as “Default”. One sensitivity run (“Default_emis”) applied the updated emission amounts of FVOCs with the original volatility distributions and SOA formation parameterization in the default complex OA scheme. The emission-related concentration differences are therefore calculated as “Default_emis” − “Default”, and the scheme-related concentration differences are calculated as “Base” − “Default_emis”. Other simulation runs such as “Zero_Biof”, “Zero_Anthro”, “Zero_BioBurn”, “Zero_Biog”) excluded OA precursor emissions from residential and biofuel, anthropogenic, biomass burning, and biogenic sources, respectively. In addition, we applied the wet deposition parameterization developed by Luo et al. (2020) in the simulation (“WDLuo”), which modifies rainout and washout parameters from the GEOS-chem default wet deposition, to explore the sensitivity of the revised OA simulation to wet-deposition settings.

2.3 Ambient observations for model evaluations

The locations of ambient observations are shown in Figure S4 in the Supplement. The OC data set consists of annual mean concentrations of OC (2016-2021) in $PM_{2.5}$ from 335 sites in various monitoring networks such as the Interagency Monitoring of Protected Visual Environments (IMPROVE) and the Chemical Speciation Network (CSN) in U.S., the European Monitoring and Evaluation Programme (EMEP), the aerosol composition network led by China National Environmental Monitoring Centre (CNEMC), and the International Network to study Deposition and Atmospheric composition in Africa (INDAAF). In addition, 58 annual mean concentrations obtained from year-long measurements between 2016 and 2021 at research sites in Asia, Africa, and Latin America are included (Table S5 in the Supplement).

https://doi.org/10.5194/egusphere-2026-3160
Preprint. Discussion started: 23 June 2026

The POA and SOA data sets include source-apportionment results from ground, shipborne, and airborne measurements by Aerodyne aerosol mass spectrometers (AMS or ACSM) (Tables S6-S8 in the Supplement). Primary and secondary OA factors were resolved, including hydrocarbon-like (HOA), cooking-related (COA), biomass-burning-related (BBOA), coal-combustion-related OA factors (CCOA), and oxygenated OA factors (OOAs). We consider the sum of HOA, BBOA, and CCOA as the observation-derived POA and the sum of OOAs as the observation-derived SOA. The COA factor is not included in the model-observation comparisons because of the lack of cooking emissions in the model. In total, 165 worldwide campaign-average surface concentrations (2015-2022) as well as the season-mean concentrations from 21 sites (2015-2019) in the Aerosol, Clouds and Trace Gases Research Infrastructure (ACTRIS) are used in model validation. All of the observation-derived POA and SOA concentrations are compared to the simulated campaign-mean or season-mean concentrations for the base year of 2018 for computation efficiency. The interannual variations of OA formation are expected to be small because of minor changes in anthropogenic emissions of organic precursors during this period in most regions (Xu et al., 2026). Anthropogenic emissions in China had a rapid decline from 2013 to 2017, followed by a slow decline afterwards. By using the middle year of observations as the simulation reference, the potential biases in model–observation comparisons are counteracted. The interannual variations of meteorology modify annual mean OA concentration within ±10% and have a minor influence on the trends (Ridley et al., 2018; Chen et al., 2024), leading to little impact on the model-observation comparisons.

Shipborne measurements we used in this study consist of four cruise tracks that occurred from April to May and October to November in 2011 and 2012 over the Atlantic Ocean between 53° N and 53° S (Huang et al., 2018). Marine and non-marine factors are resolved by the positive matrix factorization (PMF) analysis of AMS measurements during the four cruises, which showed high correlations with time series of source tracers and mass spectral patterns of identified sources. Airborne data are taken from the Wintertime Investigation of Transport, Emissions, and Reactivity (WINTER) and the Korea–United States Air Quality (KORUS-AQ) campaigns. The former was conducted in the northeastern United States from February to March in 2015 (Schroder et al., 2018), and we used the data from RF01 to RF07 for the model evaluation. The KORUS-AQ campaign was conducted over South Korea and the Yellow Sea in East Asia from May to June in 2016 (Nault et al., 2018). Model results sampled for the locations and specific date and time of each aircraft and cruise campaign are used in the comparisons.

3 Results and discussion

3.1 Model validation

Figure 2 shows the concentration differences between our updated OA simulation and the simulation with the default complex OA scheme, which are further attributed to concentration changes arising from the precursor emission update and the full-volatility-range OA scheme. The updated OA simulation results in higher OA concentrations in most continental

https://doi.org/10.5194/egusphere-2026-3160
Preprint. Discussion started: 23 June 2026

regions, especially suggesting an increase of 3 to 10 μg m^{-3} of annual-mean surface OA concentrations in polluted regions. The largest increases are present in East Asia and Central Africa, due to the net increases in both POA and SOA.

Under the newly-developed MEIC-global-FVOC emissions, the simulated POA shows a slight change in most regions (Figure 2b), suggesting most of the S/LVOC emissions are captured by traditional OC emissions. By contrast, the simulated SOA mass concentrations show 20-60% increases in East Asia, Europe, southern America, and Africa compared to the default complex OA scheme, mainly due to the increased IVOC emissions (i.e., from 6.0 to 74.1 Tg globally). The simulated POA and SOA concentrations in South Asia are however lower than the default complex OA scheme, which is attributed to relatively higher S/LVOC emissions in CEDS in that region than in MEIC-global-FVOC emissions. Overall, the precursor emission update leads to net increases of simulated OA concentrations in most continental regions.

The full-volatility-range OA scheme further increases both POA and SOA worldwide, with more increases in POA than SOA (Figure 2c). The default complex OA scheme assumes that all S/LVOC emissions fall into two surrogate bins with C^* of 1646 and 20 μg m^{-3} (Shrivastava et al., 2006). The revised OA scheme improves the representation of S/LVOC volatilities and tends to distribute more emissions into lower-volatility bins than the default scheme does, leading to increased POA mass in most continents. Then fewer S/LVOCs remain in the gas phase and hence their contributions to the SOA formation are reduced. Meanwhile, the revised OA scheme improves the representation of IVOC volatilities and their SOA yields, leading to increased SOA formation from IVOCs. In most regions, the increased SOA formation from IVOC updates is partially offset by the decreased SOA formation from S/LVOC updates, resulting in net increases of surface SOA concentrations. However, net decreases of SOA concentrations occur in some parts of Africa, South America, and North America, which are greatly affected by extreme wildfires. Because open biomass burning emissions have a greater fraction of S/LVOCs in their volatility distribution than anthropogenic emissions (Figure S5 in the Supplement), the SOA reduction from S/LVOC updates is greater than the enhancement from IVOC updates in those areas.

Figure 3 shows the comparisons of observed and simulated campaign-mean concentrations of OC, POA, and SOA in North America, Europe, and Asia. The model generally reproduces OC, POA, and SOA across regions. For POA, the normalized mean bias (NMB) values range from -0.15 to -0.01, suggesting a reasonable global estimation of the S/LVOC emissions (Figure 3b). For SOA, the NMB value is -0.14 for Asia (Figure 3c), but lower in North America (-0.28) and Europe (-0.38), suggesting unresolved underestimations in the two regions. Uncertain IVOC emissions can contribute to the underestimation of SOA in North America. The MEIC-global-FVOC shows about 20% lower VCP-related IVOC emissions in the United States than local inventories (Xu et al., 2026). Uncertain residential emissions plausibly contribute to the underestimation of SOA in Europe. There is a lack of local emission factors of S/LVOCs and IVOCs for residential biofuel burning in Europe, and emission activities of residential biofuel use are difficult to quantify there, especially in Eastern Europe (Denier van der Gon et al., 2015; Bertelsen and Vad Mathiesen, 2020). Previous studies show over 50% of OA underestimations in Europe and have attributed their underestimations to the uncertain residential wood combustion and biogenic emissions (Chebaicheb et al., 2024; Tsimpidi et al., 2025). We applied empirical scalars of 1 to 6 to increase the residential biofuel-related S/LVOC

https://doi.org/10.5194/egusphere-2026-3160
Preprint. Discussion started: 23 June 2026

emissions in some parts of Europe (Figure S2). Such residential biofuel corrections significantly improve the simulations of OC (NMB: -0.47 to -0.22), POA (NMB: -0.50 to -0.15), and SOA (NMB: -0.54 to -0.38) in Europe (Figure S6 in the Supplement), with more improvements in cold seasons (Figure 4). Additionally, insufficient mechanistic representation of SOA formation pathways may cause the underestimation at high SOA concentrations (Figure 3c). For example, aqueous and heterogeneous processes are important SOA formation pathways during haze episodes in China but remain poorly parameterized in current CTM models (Zheng et al., 2021; Gkatzelis et al., 2021). In India, high chlorine emissions may affect the SOA formation (Gunthe et al., 2021). However, neither the chlorine emissions nor the chlorine-driven pathways are well understood and sufficiently considered in the model (X. Liu et al., 2024).

It is worth mentioning that the observations for OC, POA, and SOA are still limited in high-population-density regions such as Southeast Asia, Africa, and Latin America. Panels a-c in Figure 5 show the model-observation comparisons of surface OC concentrations in those regions. The model performances are reasonable for Southeast Asia and Africa, whereas the modelled OC concentrations are much lower than the observed concentrations in Latin America. The observations in Latin America are all from urban sites, suggesting an urgent need to understand the anthropogenic sources and local emission factors. We further compared the model results to the shipborne observations. Panels e-f in Figure 5 show the simulated and observed non-marine SOA concentrations in the Atlantic Ocean (Huang et al., 2018). High concentrations of over 2 μg m^{-3} are observed in the mid-latitudes of the Northern Hemisphere and near the equator, which were influenced by long-range transport of anthropogenic pollution or open biomass burning. For other regions, the background non-marine SOA concentrations are typically below 0.5 μg m^{-3}. The model results can reproduce such variability over the Atlantic Ocean, providing a continent-wide validation of the model as well as the emission estimates. Some overestimation of the modeled non-marine SOA concentrations is present near the equator, which may be explained by underrepresented open biomass burning emissions there (Wiedinmyer et al., 2023).

Figure 6 shows the modelled vertical profiles of POA and SOA concentrations compared to the observation-derived profiles in the northeastern United States (WINTER campaign) and in East Asia (KORUS-AQ campaign). The model reproduces the observed vertical variations and concentrations of POA and SOA in the northeastern United States. For KORUS-AQ in East Asia, the model captures the vertical variations of POA and SOA, although it underestimates both POA and SOA at low altitudes. Such underestimation may result from underrepresented local emissions in the global inventory (Brewer et al., 2023; Park et al., 2021). The modelled POA concentrations are generally over 50% greater than the observations 500 m above the surface. This model bias suggests regional bias in the volatility distributions of S/LVOC emissions, which may be related to widely-used residential coal in Asia for which emission factors are limited (Shen et al., 2022). When comparing to a global data set of OA vertical profiles from aircraft campaigns, previous studies have shown that the GEOS-Chem model can capture the observed variability in OA with acceptable model biases (Pai et al., 2020; Brewer et al., 2023). These model studies did not reproduce the AMS-derived vertical profiles of POA and SOA concentrations. The traditional OA scheme with nonvolatile POA assumption would overestimate POA aloft, while the default complex OA scheme usually

https://doi.org/10.5194/egusphere-2026-3160
Preprint. Discussion started: 23 June 2026

underestimates POA (Schroder et al., 2018). The full-volatility-range OA scheme in this study shows more robust performance across different source regions and various chemical regimes for SOA production.

3.2 Surface concentrations and vertical profiles of OA

Global distributions of simulated annual-mean surface concentrations of OA, POA, and SOA from the full-volatility-range OA scheme are shown in panels a-c of Figure 7. High annual-mean OA concentrations that exceed 10 μg m^{-3} occur in China and India as well as several places in Southeast Asia, Sub-Saharan Africa, and South America. By contrast, the annual-mean OA concentrations are usually below 5 μg m^{-3} in most places in North America and Europe. In general, the SOA mass concentrations are greater than POA on the model-grid scale, and the SOA mass fractions may increase from about 30-50% in source regions to 70-90% in remote regions (Figure S7a in the Supplement).

Figure 8 shows the main sources of OA in different regions. In China, India, Europe, and Western Africa, anthropogenic sources are the predominant contributors to the OA mass, among which 50-70% of the mass is SOA. Because residential burning is the largest contributor to S/LVOCs in those regions (Xu et al., 2026), control measures on this sector would be most effective for mitigating the SOA pollution. Chen et al. (2024) show that single sector control strategy is insufficient to lower the OA levels down to 5 μg m^{-3} in China. Multi-sector control measures and clean energy replacements are urgently needed to achieve tightened air quality standards. In Southeast Asia, Southern Africa, and some parts of North America, open biomass burning is the predominant contributor to the OA mass, whereas biogenic emissions are responsible for about 30-60% of the OA mass in most parts of South America and Oceania. Under climate change, the OA concentrations in these regions may increase because of the enhanced wildfires and biogenic emissions (Pfannerstill et al., 2024; Cunningham et al., 2024).

Population exposure distributions of POA and SOA show significant differences across regions, highlighting the potential difference in POA and SOA impacts (Figure 8). For example, consistent steeper slopes of POA than SOA are present in India and China, suggesting greater reduction of population exposure per unit mass mitigation for POA. In addition, incomplete combustion is often associated with residential burning, the predominant source of POA in India and China. Studies have shown that this type of POA could have higher oxidative potential (i.e., a driver for acute health risks) than SOA (Bhattu et al., 2024; F. Liu et al., 2024). We therefore infer that the POA mitigation may bring more health co-benefits than SOA in India and China. This is very different from Europe and the United States, where SOA slopes are similar to POA's, and greater oxidative potential has been attributed to SOA (Daellenbach et al., 2020). The two factors together support the stronger association of long-term SOA exposure with cardiopulmonary mortality than POA reported by epidemiological studies (Pye et al., 2021; Pond et al., 2022). Moreover, the slopes of POA and SOA at high exposures in Southern Africa are driven by open biomass burning, and thus the majority of the population is not affected. By contrast, populations in Southeast Asia face significantly higher exposure to widespread open biomass burning, specifically by the SOA generated from these emissions.

https://doi.org/10.5194/egusphere-2026-3160
Preprint. Discussion started: 23 June 2026

The simulated zonal-mean distributions of OA, POA, and SOA concentrations are shown in panels d-f of Figure 7. The OA concentrations decrease from surface to high altitudes, reflecting the centralized precursor emissions and SOA formation near the surface. Below 600 hPa, the OA concentration is highest at the equator region, explained by high emissions of open biomass burning there (Figure S3). The Northern Hemisphere has much greater OA concentrations than the Southern Hemisphere, resulting from high anthropogenic emissions at mid-latitudes. Vertical inversions of OA concentrations occur in upper altitudes in polar regions, as is consistent with previous model findings (Tilmes et al., 2019; Lou et al., 2020). Such inversions are mainly driven by the long-range transport of SOA from mid-latitudes to high latitudes (Figure 7f). The average mass fractions of SOA may increase from over 60% at the surface to over 85% at 200 hPa (Figure S7b). Although POA contributes only 10-15% of the OA mass in upper altitudes, POA exhibits much stronger absorption than SOA (Li et al., 2025; Wang et al., 2025). Overall, a greater and more widespread absorption effect from OA is expected compared to previous estimates.

3.3 Global OA budgets

Figure 9 shows the simulated global OA burden and its comparisons to previous findings. Many previous studies treated POA as nonvolatile species and reported high POA burdens of 0.65 to 0.94 Tg (Hodzic et al., 2016; Jo et al., 2023; Lou et al., 2020; Pai et al., 2020). The nonvolatile assumption would cause large overestimations of the POA concentrations (Schroder et al., 2018; Brewer et al., 2023). The studies that considered POA as semivolatile and applied simplified parameterizations for the gas-phase partition of S/LVOCs reported much lower POA burdens of 0.03-0.24 Tg (Pye and Seinfeld, 2010; Tsimpidi et al., 2016). This discrepancy highlights the importance of a reasonable representation of the S/LVOC volatilities in modelling OA (Tsimpidi et al., 2017). Our simulations are constrained by comprehensive global data sets of POA and SOA. The estimated POA, SOA, and the total OA burdens are 0.5 Tg, 2.0 Tg, and 2.5 Tg, respectively (Table 1). Compared to the default simulations (Pye and Seinfeld, 2010), the POA burden is increased by 14.7-fold, and the SOA burden is increased by 25%. Our estimated OA burden is greater than most previous findings, but similar to the burden estimated by Lou et al. (2020), albeit with lower primary and greater secondary components.

Globally, the SOA production is 105.6 Tg yr^{-1} and represents 82% of the total OA production. This is consistent with previous top-down estimates (Heald et al., 2010; Spracklen et al., 2011). Biogenic SOA contributes to about 23% of the SOA burden (0.5 Tg), similar to the previous findings of 0.3 to 0.7 Tg (Pye and Seinfeld, 2010; Tsimpidi et al., 2017; Hodzic et al., 2016; Jo et al., 2023; Pai et al., 2020). The remaining 77% of the global SOA burden is contributed by anthropogenic and open biomass burning SOA, for which S/LVOCs and IVOCs are the main precursors and their emissions are most uncertain. Our simulations suggest S/LVOCs and IVOCs together account for 1.2 Tg of the global SOA burden, which is greater than previous findings of 0.2 Tg to 1.0 Tg. The higher SOA burden suggests that the climate impacts of SOA may have been overlooked in previous studies. Open biomass burning contributes to 46% of the SOA burden, highlighting the potential climate-driven changes of the SOA burden and distributions in the future.

https://doi.org/10.5194/egusphere-2026-3160
Preprint. Discussion started: 23 June 2026

The estimated mean lifetimes of OA, POA, and SOA are 7.1, 7.5, and 7.0 days (Figure 10a-b). The shorter lifetime of SOA than that of POA is consistent with several studies, resulting from greater wet-deposition scavenging efficiency of SOA. Wet deposition is crucial to the global OA budget, especially in remote regions (Luo et al., 2020; Gao et al., 2022). We conduct test simulations with the wet-deposition parameterization developed by Luo et al. (2020). The Luo parameterization applies a greater wet removal efficiency to reduce biases in simulated nitric acid, nitrate, and ammonium, but simultaneously decreases the estimated global OA burden by 0.8 Tg (Table S9). The global burdens of POA and SOA would decrease by 31% and 34%, respectively. Such reductions are less near sources but greater in remote regions (Figure 10c-d). The Luo parameterization may also lead to much shorter lifetimes for POA and SOA (i.e., from 7 days to 5 days in our simulations) (Figure 10a-b). Moreover, several previous studies have considered additional chemical loss pathways (e.g., via photolysis and fragmentation reactions) for SOA in the model to balance the SOA burden after implementing uncertain and empirical updates to enhance the SOA production. This implementation may lower the SOA lifetimes to less than 4 days (Hodzic et al., 2016; Lou et al., 2020). Recent studies suggest lower OA photolysis rates compared to the ones applied in the model (O'Brien and Kroll, 2019; Guan et al., 2025). Nevertheless, there is still a lack of measurements to support sophisticated parameterizations on the chemical production and removal processes for different types of OA.

4 Conclusion

In this study, we developed a new modeling framework to adopt full-volatility-range emissions of organic precursors for OA simulation in GEOS-Chem. This framework facilitates the model representation of gas-particle partitioning and SOA formation of organic precursors over a wide range of volatility and thus improves the model skills in the characterization of POA and SOA on a global scale. The new simulations show greater POA and SOA burdens across continents and suggest potentially stronger and more widespread impacts of the OA components on air quality, health, and radiation, led by both of the emission updates and the revised OA scheme. The results highlight the difference in dominant source types and population exposure distributions of POA and SOA in different regions. In India and China, POA mitigation, especially on incomplete residential burning, may still bring great health co-benefits. Long-term health-oriented air quality improvements globally need more focus on SOA, for which multi-sector control measures and clean energy replacements are necessary.

The model results are validated by a comprehensive data set including surface, airborne, and shipborne measurements. One caveat is that the PMF-derived POA and SOA concentrations are not identical to the modelled POA and SOA. We think the comparisons between the sum of HOA, CCOA, COA, and BBOA to the modeled POA and the sum of OOAs to the modeled SOA are meaningful because (1) the PMF POA factors cover the main anthropogenic source types whose emissions are represented by the new inventory except cooking; (2) the PMF OOA factors represent SOA from various precursors with different photochemical ages as well as aqueous SOA (Jimenez et al., 2009; Chen et al., 2015; Zheng et al., 2023), and the modelled SOA is the sum of biogenic SOA, aromatic SOA, IVOC SOA, S/LVOC SOA, and key aqueous SOA which covers all important precursors and their photooxidation and aqueous processes. The mass fraction of COA on a regional or global

https://doi.org/10.5194/egusphere-2026-3160
Preprint. Discussion started: 23 June 2026

scale should be small. The PMF-derived SOA includes heterogenous aging of POA which may explain a part of the underestimation of modeled SOA but expected to be small given the good comparisons aloft and in remote regions.

Although we have updated the OA scheme with continuous volatility bins and better SOA yields, the SOA scheme remains as a volatility-lumped and yield-based approach. Model accuracy is limited when exploring local temporal variations (Woody et al., 2016; Miao et al., 2020; Oak et al., 2022; Chen et al., 2024). Advanced measurements on local emission factors of full-volatility-range organic precursors from anthropogenic sources as well as the simultaneous quantification of the total organic carbon mass to constrain the S/LVOC emissions are crucial but limited, particularly for Europe and India. OA source apportionment data are rare in Southeast Asia, Africa, and Latin America, calling for more ambient measurements there. There is still room for improving the yield parameterization. The IVOC-SOA yields in this study depend on only the IVOC precursor volatilities, which should include justifications on their molecular structure and the NO_x level (Tkacik et al., 2012; Lu et al., 2020; Manavi and Pandis, 2022). Moreover, the nonlinear response of SOA formation to global warming is largely unknown. The temperature dependence of organic emissions needs to be considered in the model (Wu et al., 2024; Pfannerstill et al., 2024). Our results highlight the high contribution of open biomass burning to the global SOA burden. Significant changes in SOA production are expected in the future because of the reduction of anthropogenic emissions driven by tightened regional air quality standards (e.g., in China) and the intensified wildfires. The difference in global annual emissions of OC from open biomass burning is over 100% among commonly used emission inventories and much higher regionally (Carter et al., 2020; Wiedinmyer et al., 2023). It is important to further constrain open biomass burning emissions and understand the chemical conversion of biomass burning plumes. Finally, the simulated OA burden is sensitive to the parameterization of wet deposition, calling for more measurements of the deposition fluxes of OA and its components.

Data availability

The airborne measurement data and PMF results of the WINTER and KORUS-AQ campaigns are downloaded from UCAR/NCAR - Earth Observing Laboratory (https://doi.org/10.5065/D6MC8XT8) and are provided by the dataset of Brewer et al. (2023) (https://doi.org/10.7910/DVN/IDWE39), respectively. IMPROVE and CSN data are downloaded from http://views.cira.colostate.edu/fed/. EMEP and INDAAF data are downloaded from https://ebas-data.nilu.no/ and https://indaaf.obs-mip.fr/, respectively. Surface measurement data that gathered from literatures are listed in the Supplement. Other data presented in this paper are available upon request to the corresponding author.

Author contributions

Q.C. designed the study. R.X., J.L., and G.G. provided the MEIC-global-FVOC emission inventory. R.M. and R.X. prepared the data set of surface OC measurements. R.M., S.X., H.W., Y.Z., and S.L. prepared the data set of global AMS and ACSM

https://doi.org/10.5194/egusphere-2026-3160
Preprint. Discussion started: 23 June 2026

measurements. K.R.D., I.E.H., and A.S.H.P. provided the measurement data from ACTRIS network. S.H. provided the data of shipborne measurements. R.M. developed the model scheme and performed the model simulations. R.M, Q.C., R.X., and I.E.H. analyzed the model data. R.M, Q.C., R.X., J.J., I.E.H., M.S., C.G., G.B., V.A.K. and A.P.T. discussed the model results. R.M. and Q.C. wrote the paper with comments from all the other authors.

Competing interests

At least one of the (co-)authors is a member of the editorial board of Atmospheric Chemistry and Physics.

Acknowledgments

This work was supported by the National Natural Science Foundation of China (grant nos. 42525502, 42407147, and 42377088) and the 111 Project of Urban Air Pollution and Health Effects (B20009). Manish Shrivastava acknowledges support from the US Department of Energy (DOE) Biological and Environmental Research (BER) through its Atmospheric System Research (ASR) program. The Pacific Northwest National Laboratory is operated by Battelle Memorial Institute for the US DOE under Contract DE-AC05-76RL01830. We acknowledge the support by the ACTRIS related Emissions Reduction Monitoring Infrastructure (ERMI) Programme in Romania and Czech-Swiss State-of-the-Art Characterization of Atmosphere: Aerosols and Reactive Trace Gases (SACA-ACTRIS). The authors gratefully acknowledge Prof. Qiang Zhang and the MEIC team for their support on emission inventory developments.

References

Bertelsen, N., and Vad Mathiesen, B.: EU-28 Residential Heat Supply and Consumption: Historical Development and Status, Energies, 13, 1894, 2020.

Bey, I., Jacob, D. J., Yantosca, R. M., Logan, J. A., Field, B. D., Fiore, A. M., Li, Q. B., Liu, H. G. Y., Mickley, L. J., and Schultz, M. G.: Global modeling of tropospheric chemistry with assimilated meteorology: Model description and evaluation, J. Geophys. Res. Atmos., 106, 23073-23095, https://doi.org/10.1029/2001JD000807, 2001.

Bhattu, D., Tripathi, S. N., Bhowmik, H. S., Moschos, V., Lee, C. P., Rauber, M., Salazar, G., Abbaszade, G., Cui, T., Slowik, J. G., Vats, P., Mishra, S., Lalchandani, V., Satish, R., Rai, P., Casotto, R., Tobler, A., Kumar, V., Hao, Y., Qi, L., Khare, P., Manousakas, M. I., Wang, Q., Han, Y., Tian, J., Darfeuil, S., Minguillon, M. C., Hueglin, C., Conil, S., Rastogi, N., Srivastava, A. K., Ganguly, D., Bjelic, S., Canonaco, F., Schnelle-Kreis, J., Dominutti, P. A., Jaffrezo, J.-L., Szidat, S., Chen, Y., Cao, J., Baltensperger, U., Uzu, G., Daellenbach, K. R., El Haddad, I., and Prévôt, A. S. H.: Local incomplete combustion emissions define the $PM_{2.5}$ oxidative potential in Northern India, Nat. Commun., 15, 3517, https://doi.org/10.1038/s41467-024-47785-5, 2024.

Brewer, J. F., Jacob, D. J., Jathar, S. H., He, Y., Akherati, A., Zhai, S., Jo, D. S., Hodzic, A., Nault, B. A., Campuzano-Jost, P., Jimenez, J. L., Park, R. J., Oak, Y. J., and Liao, H.: A Scheme for Representing Aromatic Secondary Organic Aerosols in Chemical Transport Models: Application to Source Attribution of Organic Aerosols Over South Korea During the KORUS-AQ Campaign, J. Geophys. Res. Atmos., 128, e2022JD037257, https://doi.org/10.1029/2022JD037257, 2023.

https://doi.org/10.5194/egusphere-2026-3160
Preprint. Discussion started: 23 June 2026

Carter, T. S., Heald, C. L., Jimenez, J. L., Campuzano-Jost, P., Kondo, Y., Moteki, N., Schwarz, J. P., Wiedinmyer, C., Darmenov, A. S., da Silva, A. M., and Kaiser, J. W.: How emissions uncertainty influences the distribution and radiative impacts of smoke from fires in North America, Atmos. Chem. Phys., 20, 2073-2097, https://doi.org/10.5194/acp-20-2073-2020, 2020.

Chan, A. W. H., Kautzman, K. E., Chhabra, P. S., Surratt, J. D., Chan, M. N., Crounse, J. D., Kurten, A., Wennberg, P. O., Flagan, R. C., and Seinfeld, J. H.: Secondary organic aerosol formation from photooxidation of naphthalene and alkylnaphthalenes: implications for oxidation of intermediate volatility organic compounds (IVOCs), Atmos. Chem. Phys., 9, 3049-3060, https://doi.org/10.5194/acp-9-3049-2009, 2009.

Chang, X., Zhao, B., Zheng, H., Wang, S., Cai, S., Guo, F., Gui, P., Huang, G., Wu, D., Han, L., Xing, J., Man, H., Hu, R., Liang, C., Xu, Q., Qiu, X., Ding, D., Liu, K., Han, R., Robinson, A. L., and Donahue, N. M.: Full-volatility emission framework corrects missing and underestimated secondary organic aerosol sources, One Earth, 5, 403-412, https://doi.org/10.1016/j.oneear.2022.03.015, 2022.

Chebaicheb, H., de Brito, J. F., Amodeo, T., Couvidat, F., Petit, J. E., Tison, E., Abbou, G., Baudic, A., Chatain, M., Chazeau, B., Marchand, N., Falhun, R., Francony, F., Ratier, C., Grenier, D., Vidaud, R., Zhang, S., Gille, G., Meunier, L., Marchand, C., Riffault, V., and Favez, O.: Multiyear high-temporal-resolution measurements of submicron aerosols at 13 French urban sites: data processing and chemical composition, Earth Syst. Sci. Data, 16, 5089-5109, https://doi.org/10.5194/essd-16-5089-2024, 2024.

Chen, Q., Heald, C. L., Jimenez, J. L., Canagaratna, M. R., Zhang, Q., He, L. Y., Huang, X. F., Campuzano-Jost, P., Palm, B. B., Poulain, L., Kuwata, M., Martin, S. T., Abbatt, J. P. D., Lee, A. K. Y., and Liggio, J.: Elemental composition of organic aerosol: The gap between ambient and laboratory measurements, Geophys. Res. Lett., 42, 4182-4189, https://doi.org/10.1002/2015GL063693, 2015.

Chen, Q., Miao, R., Geng, G., Shrivastava, M., Dao, X., Xu, B., Sun, J., Zhang, X., Liu, M., Tang, G., Tang, Q., Hu, H., Huang, R.-J., Wang, H., Zheng, Y., Qin, Y., Guo, S., Hu, M., and Zhu, T.: Widespread 2013-2020 decreases and reduction challenges of organic aerosol in China, Nat. Commun., 15, 4465, https://doi.org/10.1038/s41467-024-48902-0, 2024.

Chung, S. H., and Seinfeld, J. H.: Global distribution and climate forcing of carbonaceous aerosols, J. Geophys. Res. Atmos., 107, 4407, https://doi.org/10.1029/2001JD001397, 2002.

Cunningham, C. X., Williamson, G. J., and Bowman, D. M. J. S.: Increasing frequency and intensity of the most extreme wildfires on Earth, Nat. Ecol. Evol., 8, 1420-1425, https://doi.org/10.1038/s41559-024-02452-2, 2024.

Daellenbach, K. R., Uzu, G., Jiang, J., Cassagnes, L.-E., Leni, Z., Vlachou, A., Stefenelli, G., Canonaco, F., Weber, S., Segers, A., Kuenen, J. J. P., Schaap, M., Favez, O., Albinet, A., Aksoyoglu, S., Dommen, J., Baltensperger, U., Geiser, M., El Haddad, I., Jaffrezo, J.-L., and Prévôt, A. S. H.: Sources of particulate-matter air pollution and its oxidative potential in Europe, Nature, 587, 414-419, https://doi.org/10.1038/s41586-020-2902-8, 2020.

Denier van der Gon, H. A. C., Bergström, R., Fountoukis, C., Johansson, C., Pandis, S. N., Simpson, D., and Visschedijk, A. J. H.: Particulate emissions from residential wood combustion in Europe – revised estimates and an evaluation, Atmos. Chem. Phys., 15, 6503-6519, https://doi.org/10.5194/acp-15-6503-2015, 2015.

Donahue, N. M., Kroll, J. H., Pandis, S. N., and Robinson, A. L.: A two-dimensional volatility basis set – Part 2: Diagnostics of organic-aerosol evolution, Atmos. Chem. Phys., 12, 615-634, https://doi.org/10.5194/acp-12-615-2012, 2012.

Fountoukis, C., and Nenes, A.: ISORROPIA II: a computationally efficient thermodynamic equilibrium model for K^+-Ca^{2+}-Mg^{2+}-NH_4^+-Na^+-SO_4^{2-}-NO_3^--Cl^--H_2O aerosols, Atmos. Chem. Phys., 7, 4639-4659, https://doi.org/10.5194/acp-7-4639-2007, 2007.

Gao, C. Y., Heald, C. L., Katich, J. M., Luo, G., and Yu, F.: Remote Aerosol Simulated During the Atmospheric Tomography (ATom) Campaign and Implications for Aerosol Lifetime, J. Geophys. Res. Atmos., 127, e2022JD036524, https://doi.org/https://doi.org/10.1029/2022JD036524, 2022.

https://doi.org/10.5194/egusphere-2026-3160
Preprint. Discussion started: 23 June 2026

Geng, G., Liu, Y., Liu, Y., Liu, S., Cheng, J., Yan, L., Wu, N., Hu, H., Tong, D., Zheng, B., Yin, Z., He, K., and Zhang, Q.: Efficacy of China's clean air actions to tackle PM2.5 pollution between 2013 and 2020, Nat. Geosci., 17, 987-994, https://doi.org/10.1038/s41561-024-01540-z, 2024.

Gkatzelis, G. I., Papanastasiou, D. K., Karydis, V. A., Hohaus, T., Liu, Y., Schmitt, S. H., Schlag, P., Fuchs, H., Novelli, A., Chen, Q., Cheng, X., Broch, S., Dong, H., Holland, F., Li, X., Liu, Y., Ma, X., Reimer, D., Rohrer, F., Shao, M., Tan, Z., Taraborrelli, D., Tillmann, R., Wang, H., Wang, Y., Wu, Y., Wu, Z., Zeng, L., Zheng, J., Hu, M., Lu, K., Hofzumahaus, A., Zhang, Y., Wahner, A., and Kiendler-Scharr, A.: Uptake of Water-soluble Gas-phase Oxidation Products Drives Organic Particulate Pollution in Beijing, Geophys. Res. Lett., 48, e2020GL091351, https://doi.org/10.1029/2020GL091351, 2021.

Guan, J., Solomon, S., Murphy, D. M., Stone, K., Yu, P., Kinnison, D., Schill, G. P., Tilmes, S., and Lawler, M. J.: Limited Long-Term Photolysis of Stratospheric Organic Aerosols With Implications for CESM Modeling, J. Adv. Model. Earth Syst., 17, e2025MS005084, https://doi.org/10.1029/2025MS005084, 2025.

Guenther, A. B., Jiang, X., Heald, C. L., Sakulyanontvittaya, T., Duhl, T., Emmons, L. K., and Wang, X.: The Model of Emissions of Gases and Aerosols from Nature version 2.1 (MEGAN2.1): an extended and updated framework for modeling biogenic emissions, Geosci. Model Dev., 5, 1471-1492, https://doi.org/10.5194/gmd-5-1471-2012, 2012.

Gunthe, S. S., Liu, P., Panda, U., Raj, S. S., Sharma, A., Darbyshire, E., Reyes-Villegas, E., Allan, J., Chen, Y., Wang, X., Song, S., Pöhlker, M. L., Shi, L., Wang, Y., Kommula, S. M., Liu, T., Ravikrishna, R., McFiggans, G., Mickley, L. J., Martin, S. T., Pöschl, U., Andreae, M. O., and Coe, H.: Enhanced aerosol particle growth sustained by high continental chlorine emission in India, Nat. Geosci., 14, 77-84, https://doi.org/10.1038/s41561-020-00677-x, 2021.

Hallquist, M., Wenger, J. C., Baltensperger, U., Rudich, Y., Simpson, D., Claeys, M., Dommen, J., Donahue, N. M., George, C., Goldstein, A. H., Hamilton, J. F., Herrmann, H., Hoffmann, T., Iinuma, Y., Jang, M., Jenkin, M. E., Jimenez, J. L., Kiendler-Scharr, A., Maenhaut, W., McFiggans, G., Mentel, T. F., Monod, A., Prévôt, A. S. H., Seinfeld, J. H., Surratt, J. D., Szmigielski, R., and Wildt, J.: The formation, properties and impact of secondary organic aerosol: current and emerging issues, Atmos. Chem. Phys., 9, 5155-5236, https://doi.org/10.5194/acp-9-5155-2009, 2009.

Heald, C. L., Ridley, D. A., Kreidenweis, S. M., and Drury, E. E.: Satellite observations cap the atmospheric organic aerosol budget, Geophys. Res. Lett., 37, L24808, https://doi.org/10.1029/2010gl045095, 2010.

Heald, C. L., Ridley, D. A., Kroll, J. H., Barrett, S. R. H., Cady-Pereira, K. E., Alvarado, M. J., and Holmes, C. D.: Contrasting the direct radiative effect and direct radiative forcing of aerosols, Atmos. Chem. Phys., 14, 5513-5527, https://doi.org/10.5194/acp-14-5513-2014, 2014.

Hodzic, A., Kasibhatla, P. S., Jo, D. S., Cappa, C. D., Jimenez, J. L., Madronich, S., and Park, R. J.: Rethinking the global secondary organic aerosol (SOA) budget: stronger production, faster removal, shorter lifetime, Atmos. Chem. Phys., 16, 7917-7941, https://doi.org/10.5194/acp-16-7917-2016, 2016.

Hoesly, R. M., Smith, S. J., Feng, L., Klimont, Z., Janssens-Maenhout, G., Pitkanen, T., Seibert, J. J., Vu, L., Andres, R. J., Bolt, R. M., Bond, T. C., Dawidowski, L., Kholod, N., Kurokawa, J., Li, M., Liu, L., Lu, Z., Moura, M. C. P., O'Rourke, P. R., and Zhang, Q.: Historical (1750-2014) anthropogenic emissions of reactive gases and aerosols from the Community Emissions Data System (CEDS), Geosci. Model Dev., 11, 369-408, https://doi.org/10.5194/gmd-11-369-2018, 2018.

Huang, L., Zhao, B., Wang, S., Chang, X., Klimont, Z., Huang, G., Zheng, H., and Hao, J.: Global Anthropogenic Emissions of Full-Volatility Organic Compounds, Environ. Sci. Technol., 57, 16435-16445, https://doi.org/10.1021/acs.est.3c04106, 2023.

Huang, S., Wu, Z., Poulain, L., van Pinxteren, M., Merkel, M., Assmann, D., Herrmann, H., and Wiedensohler, A.: Source apportionment of the organic aerosol over the Atlantic Ocean from 53°N to 53°S: significant contributions from marine emissions and long-range transport, Atmos. Chem. Phys., 18, 18043-18062, https://doi.org/10.5194/acp-18-18043-2018, 2018.

https://doi.org/10.5194/egusphere-2026-3160
Preprint. Discussion started: 23 June 2026

Hudman, R. C., Moore, N. E., Mebust, A. K., Martin, R. V., Russell, A. R., Valin, L. C., and Cohen, R. C.: Steps towards a mechanistic model of global soil nitric oxide emissions: implementation and space based-constraints, Atmos. Chem. Phys., 12, 7779-7795, https://doi.org/10.5194/acp-12-7779-2012, 2012.

Jathar, S. H., Farina, S. C., Robinson, A. L., and Adams, P. J.: The influence of semi-volatile and reactive primary emissions on the abundance and properties of global organic aerosol, Atmos. Chem. Phys., 11, 7727-7746, https://doi.org/10.5194/acp-11-7727-2011, 2011.

Jiang, J., Aksoyoglu, S., El-Haddad, I., Ciarelli, G., Denier van der Gon, H. A. C., Canonaco, F., Gilardoni, S., Paglione, M., Minguillón, M. C., Favez, O., Zhang, Y., Marchand, N., Hao, L., Virtanen, A., Florou, K., O'Dowd, C., Ovadnevaite, J., Baltensperger, U., and Prévôt, A. S. H.: Sources of organic aerosols in Europe: a modeling study using CAMx with modified volatility basis set scheme, Atmos. Chem. Phys., 19, 15247-15270, https://doi.org/10.5194/acp-19-15247-2019, 2019.

Jimenez, J. L., Canagaratna, M. R., Donahue, N. M., Prevot, A. S., Zhang, Q., Kroll, J. H., DeCarlo, P. F., Allan, J. D., Coe, H., Ng, N. L., Aiken, A. C., Docherty, K. S., Ulbrich, I. M., Grieshop, A. P., Robinson, A. L., Duplissy, J., Smith, J. D., Wilson, K. R., Lanz, V. A., Hueglin, C., Sun, Y. L., Tian, J., Laaksonen, A., Raatikainen, T., Rautiainen, J., Vaattovaara, P., Ehn, M., Kulmala, M., Tomlinson, J. M., Collins, D. R., Cubison, M. J., Dunlea, E. J., Huffman, J. A., Onasch, T. B., Alfarra, M. R., Williams, P. I., Bower, K., Kondo, Y., Schneider, J., Drewnick, F., Borrmann, S., Weimer, S., Demerjian, K., Salcedo, D., Cottrell, L., Griffin, R., Takami, A., Miyoshi, T., Hatakeyama, S., Shimono, A., Sun, J. Y., Zhang, Y. M., Dzepina, K., Kimmel, J. R., Sueper, D., Jayne, J. T., Herndon, S. C., Trimborn, A. M., Williams, L. R., Wood, E. C., Middlebrook, A. M., Kolb, C. E., Baltensperger, U., and Worsnop, D. R.: Evolution of Organic Aerosols in the Atmosphere, Science, 326, 1525-1529, https://doi.org/10.1126/science.1180353, 2009.

Jo, D. S., Park, R. J., Kim, M. J., and Spracklen, D. V.: Effects of chemical aging on global secondary organic aerosol using the volatility basis set approach, Atmos. Environ., 81, 230-244, https://doi.org/10.1016/j.atmosenv.2013.08.055, 2013.

Jo, D. S., Nault, B. A., Tilmes, S., Gettelman, A., McCluskey, C. S., Hodzic, A., Henze, D. K., Nawaz, M. O., Fung, K. M., and Jimenez, J. L.: Global Health and Climate Effects of Organic Aerosols from Different Sources, Environ. Sci. Technol., 57, 13793-13807, https://doi.org/10.1021/acs.est.3c02823, 2023.

Li, Y., Fu, T.-M., Yu, J. Z., Zhang, A., Yu, X., Ye, J., Zhu, L., Shen, H., Wang, C., Yang, X., Tao, S., Chen, Q., Li, Y., Li, L., Che, H., and Heald, C. L.: Nitrogen dominates global atmospheric organic aerosol absorption, Science, 387, 989-995, https://doi.org/doi:10.1126/science.adr4473, 2025.

Lin, G., Penner, J. E., Flanner, M. G., Sillman, S., Xu, L., and Zhou, C.: Radiative forcing of organic aerosol in the atmosphere and on snow: Effects of SOA and brown carbon, J. Geophys. Res. Atmos., 119, 7453-7476, https://doi.org/10.1002/2013JD021186, 2014.

Liu, F., Yang, X., Xu, W., Verma, V., Wang, Z., Chen, C., He, Y., Yang, L., Yang, Y., Sun, Y., and He, C.: Resolving Organic Aerosol Components Contributing to the Oxidative Potential of PM2.5 in the North China Plain, J. Geophys. Res. Atmos., 129, e2024JD040840, https://doi.org/10.1029/2024JD040840, 2024.

Liu, H., Jacob, D. J., Bey, I., and Yantosca, R. M.: Constraints from ^{210}Pb and ^{7}Be on wet deposition and transport in a global three-dimensional chemical tracer model driven by assimilated meteorological fields, J. Geophys. Res. Atmos., 106, 12109-12128, https://doi.org/10.1029/2000JD900839, 2001.

Liu, X., Liu, L., Zhang, B., Liu, P., Huang, R.-J., Hildebrandt Ruiz, L., Miao, R., Chen, Q., and Wang, X.: Modeling the Global Impact of Chlorine Chemistry on Secondary Organic Aerosols, Environ. Sci. Technol., 58, 23064-23074, https://doi.org/10.1021/acs.est.4c05037, 2024.

Lou, S. J., Shrivastava, M., Easter, R. C., Yang, Y., Ma, P. L., Wang, H. L., Cubison, M. J., Campuzano-Jost, P., Jimenez, J. L., Zhang, Q., Rasch, P. J., Shilling, J. E., Zelenyuk, A., Dubey, M., Cameron-Smith, P., Martin, S. T., Schneider, J., and Schulz, C.: New SOA Treatments Within the Energy Exascale Earth System Model (E3SM): Strong Production and Sinks Govern Atmospheric SOA Distributions and Radiative Forcing, J. Adv. Model. Earth Syst., 12, e2020MS002266, https://doi.org/10.1029/2020MS002266, 2020.

https://doi.org/10.5194/egusphere-2026-3160
Preprint. Discussion started: 23 June 2026

Lu, Q., Murphy, B. N., Qin, M., Adams, P. J., Zhao, Y., Pye, H. O. T., Efstathiou, C., Allen, C., and Robinson, A. L.: Simulation of organic aerosol formation during the CalNex study: updated mobile emissions and secondary organic aerosol parameterization for intermediate-volatility organic compounds, Atmos. Chem. Phys., 20, 4313-4332, https://doi.org/10.5194/acp-20-4313-2020, 2020.

Luo, G., Yu, F., and Moch, J. M.: Further improvement of wet process treatments in GEOS-Chem v12.6.0: impact on global distributions of aerosols and aerosol precursors, Geosci. Model Dev., 13, 2879-2903, https://doi.org/10.5194/gmd-13-2879-2020, 2020.

Manavi, S. E. I., and Pandis, S. N.: A lumped species approach for the simulation of secondary organic aerosol production from intermediate-volatility organic compounds (IVOCs): application to road transport in PMCAMx-iv (v1.0), Geosci. Model Dev., 15, 7731-7749, https://doi.org/10.5194/gmd-15-7731-2022, 2022.

Manavi, S. E. I., and Pandis, S. N.: Contribution of intermediate-volatility organic compounds from on-road transport to secondary organic aerosol levels in Europe, Atmos. Chem. Phys., 24, 891-909, https://doi.org/10.5194/acp-24-891-2024, 2024.

Marais, E. A., Jacob, D. J., Jimenez, J. L., Campuzano-Jost, P., Day, D. A., Hu, W., Krechmer, J., Zhu, L., Kim, P. S., Miller, C. C., Fisher, J. A., Travis, K., Yu, K., Hanisco, T. F., Wolfe, G. M., Arkinson, H. L., Pye, H. O. T., Froyd, K. D., Liao, J., and McNeill, V. F.: Aqueous-phase mechanism for secondary organic aerosol formation from isoprene: application to the southeast United States and co-benefit of SO_2 emission controls, Atmos. Chem. Phys., 16, 1603-1618, https://doi.org/10.5194/acp-16-1603-2016, 2016.

McDuffie, E. E., Smith, S. J., O'Rourke, P., Tibrewal, K., Venkataraman, C., Marais, E. A., Zheng, B., Crippa, M., Brauer, M., and Martin, R. V.: A global anthropogenic emission inventory of atmospheric pollutants from sector- and fuel-specific sources (1970–2017): an application of the Community Emissions Data System (CEDS), Earth Syst. Sci. Data, 12, 3413-3442, https://doi.org/10.5194/essd-12-3413-2020, 2020.

Miao, R., Chen, Q., Zheng, Y., Cheng, X., Sun, Y., Palmer, P. I., Shrivastava, M., Guo, J., Zhang, Q., Liu, Y., Tan, Z., Ma, X., Chen, S., Zeng, L., Lu, K., and Zhang, Y.: Model bias in simulating major chemical components of $PM_{2.5}$ in China, Atmos. Chem. Phys., 20, 12265-12284, https://doi.org/10.5194/acp-20-12265-2020, 2020.

Miao, R., Chen, Q., Shrivastava, M., Chen, Y., Zhang, L., Hu, J., Zheng, Y., and Liao, K.: Process-based and observation-constrained SOA simulations in China: the role of semivolatile and intermediate-volatility organic compounds and OH levels, Atmos. Chem. Phys., 21, 16183-16201, https://doi.org/10.5194/acp-21-16183-2021, 2021.

Murphy, B. N., Woody, M. C., Jimenez, J. L., Carlton, A. M. G., Hayes, P. L., Liu, S., Ng, N. L., Russell, L. M., Setyan, A., Xu, L., Young, J., Zaveri, R. A., Zhang, Q., and Pye, H. O. T.: Semivolatile POA and parameterized total combustion SOA in CMAQv5.2: impacts on source strength and partitioning, Atmos. Chem. Phys., 17, 11107-11133, https://doi.org/10.5194/acp-17-11107-2017, 2017.

Nault, B. A., Campuzano-Jost, P., Day, D. A., Schroder, J. C., Anderson, B., Beyersdorf, A. J., Blake, D. R., Brune, W. H., Choi, Y., Corr, C. A., de Gouw, J. A., Dibb, J., DiGangi, J. P., Diskin, G. S., Fried, A., Huey, L. G., Kim, M. J., Knote, C. J., Lamb, K. D., Lee, T., Park, T., Pusede, S. E., Scheuer, E., Thornhill, K. L., Woo, J. H., and Jimenez, J. L.: Secondary organic aerosol production from local emissions dominates the organic aerosol budget over Seoul, South Korea, during KORUS-AQ, Atmos. Chem. Phys., 18, 17769-17800, https://doi.org/10.5194/acp-18-17769-2018, 2018.

O'Brien, R. E., and Kroll, J. H.: Photolytic Aging of Secondary Organic Aerosol: Evidence for a Substantial Photo-Recalcitrant Fraction, J. Phys. Chem. Lett., 10, 4003-4009, https://doi.org/10.1021/acs.jpclett.9b01417, 2019.

Oak, Y. J., Park, R. J., Jo, D. S., Hodzic, A., Jimenez, J. L., Campuzano-Jost, P., Nault, B. A., Kim, H., Kim, H., Ha, E. S., Song, C. K., Yi, S. M., Diskin, G. S., Weinheimer, A. J., Blake, D. R., Wisthaler, A., Shim, M., and Shin, Y.: Evaluation of Secondary Organic Aerosol (SOA) Simulations for Seoul, Korea, J. Adv. Model. Earth Syst., 14, e2021MS002760, https://doi.org/10.1029/2021MS002760, 2022.

https://doi.org/10.5194/egusphere-2026-3160
Preprint. Discussion started: 23 June 2026

Pai, S. J., Heald, C. L., Pierce, J. R., Farina, S. C., Marais, E. A., Jimenez, J. L., Campuzano-Jost, P., Nault, B. A., Middlebrook, A. M., Coe, H., Shilling, J. E., Bahreini, R., Dingle, J. H., and Vu, K.: An evaluation of global organic aerosol schemes using airborne observations, Atmos. Chem. Phys., 20, 2637-2665, https://doi.org/10.5194/acp-20-2637-2020, 2020.

Park, R. J., Oak, Y. J., Emmons, L. K., Kim, C.-H., Pfister, G. G., Carmichael, G. R., Saide, P. E., Cho, S.-Y., Kim, S., Woo, J.-H., Crawford, J. H., Gaubert, B., Lee, H. J., Park, S.-Y., Jo, Y.-J., Gao, M., Tang, B. M., Stanier, C. O., Shin, S. S., Park, H. Y., Bae, C., and Kim, E.: Multi-model intercomparisons of air quality simulations for the KORUS-AQ campaign, Elementa-Sci. Anthrop., 9, https://doi.org/10.1525/elementa.2021.00139, 2021.

Pfannerstill, E. Y., Arata, C., Zhu, Q., Schulze, B. C., Ward, R., Woods, R., Harkins, C., Schwantes, R. H., Seinfeld, J. H., Bucholtz, A., Cohen, R. C., and Goldstein, A. H.: Temperature-dependent emissions dominate aerosol and ozone formation in Los Angeles, Science, 384, 1324-1329, https://doi.org/doi:10.1126/science.adg8204, 2024.

Pond, Z. A., Hernandez, C. S., Adams, P. J., Pandis, S. N., Garcia, G. R., Robinson, A. L., Marshall, J. D., Burnett, R., Skyllakou, K., Garcia Rivera, P., Karnezi, E., Coleman, C. J., and Pope, C. A., III: Cardiopulmonary Mortality and Fine Particulate Air Pollution by Species and Source in a National U.S. Cohort, Environ. Sci. Technol., 56, 7214-7223, https://doi.org/10.1021/acs.est.1c04176, 2022.

Presto, A. A., Miracolo, M. A., Donahue, N. M., and Robinson, A. L.: Secondary Organic Aerosol Formation from High-NO_x Photo-Oxidation of Low Volatility Precursors: *n*-Alkanes, Environ. Sci. Technol., 44, 2029-2034, https://doi.org/10.1021/es903712r, 2010.

Pye, H. O. T., Liao, H., Wu, S., Mickley, L. J., Jacob, D. J., Henze, D. K., and Seinfeld, J. H.: Effect of changes in climate and emissions on future sulfate-nitrate-ammonium aerosol levels in the United States, J. Geophys. Res. Atmos., 114, https://doi.org/10.1029/2008JD010701, 2009.

Pye, H. O. T., Chan, A. W. H., Barkley, M. P., and Seinfeld, J. H.: Global modeling of organic aerosol: the importance of reactive nitrogen (NO_x and NO_3), Atmos. Chem. Phys., 10, 11261-11276, https://doi.org/10.5194/acp-10-11261-2010, 2010.

Pye, H. O. T., and Seinfeld, J. H.: A global perspective on aerosol from low-volatility organic compounds, Atmos. Chem. Phys., 10, 4377-4401, https://doi.org/10.5194/acp-10-4377-2010, 2010.

Pye, H. O. T., Ward-Caviness, C. K., Murphy, B. N., Appel, K. W., and Seltzer, K. M.: Secondary organic aerosol association with cardiorespiratory disease mortality in the United States, Nat. Commun., 12, 7215, https://doi.org/10.1038/s41467-021-27484-1, 2021.

Pye, H. O. T., Place, B. K., Murphy, B. N., Seltzer, K. M., D'Ambro, E. L., Allen, C., Piletic, I. R., Farrell, S., Schwantes, R. H., Coggon, M. M., Saunders, E., Xu, L., Sarwar, G., Hutzell, W. T., Foley, K. M., Pouliot, G., Bash, J., and Stockwell, W. R.: Linking gas, particulate, and toxic endpoints to air emissions in the Community Regional Atmospheric Chemistry Multiphase Mechanism (CRACMM), Atmos. Chem. Phys., 23, 5043-5099, https://doi.org/10.5194/acp-23-5043-2023, 2023.

Ridley, D. A., Heald, C. L., Ridley, K. J., and Kroll, J. H.: Causes and consequences of decreasing atmospheric organic aerosol in the United States, Proc. Natl. Acad. Sci. U. S. A., 115, 290-295, https://doi.org/10.1073/pnas.1700387115, 2018.

Riipinen, I., Talvinen, S., Chassaing, A., Georgakaki, P., Li, X., García-Pando, C. P., Bergman, T., Kommula, S. M., Proske, U., Gkouvousis, A., Tsimpidi, A. P., Chatziparaschos, M., Neuberger, A., Karydis, V. A., Calderón, S. M., Romakkaniemi, S., Partridge, D. G., Khadir, T., Dada, L., van Noije, T., Decesari, S., Seland, Ø., Zieger, P., Bender, F., Carslaw, K., Cermak, J., Costa-Surós, M., Gonçalves Ageitos, M., Gramlich, Y., Haugvaldstad, O. W., Holopainen, E., Hoose, C., Jorba, O., Kakavas, S., Kanakidou, M., Kokkola, H., Krejci, R., Kühn, T., Kulmala, M., Le Sager, P., Makkonen, R., Manavi, S. E. I., Mentel, T. F., Milousis, A., Myriokefalitakis, S., Nenes, A., Nieminen, T., Pandis, S. N., Patoulias, D., Petäjä, T., Quaas, J., Regayre, L., Scholz, S. M. C., Schulz, M., Skyllakou, K., Sousse, R., Stier, P., Thomas, M. A., Villinger, J. T., Virtanen, A., Wyser, K., and Ekman, A. M. L.: Treatment of Key Aerosol and Cloud Processes in Earth System Models – Recommendations from the FORCeS Project, Tellus B: Chem. Phys. Meteorol., https://doi.org/10.16993/tellusb.1883, 2026.

https://doi.org/10.5194/egusphere-2026-3160
Preprint. Discussion started: 23 June 2026

Scholz, S. M. C., Karydis, V. A., Gkatzelis, G. I., Fuchs, H., Pandis, S. N., and Tsimpidi, A. P.: Incorporation of lumped IVOC emissions into the ORACLE model (V1.1): a multi-product framework for assessing global SOA formation from internal combustion engines, Geosci. Model Dev., 18, 10119-10142, https://doi.org/10.5194/gmd-18-10119-2025, 2025.

Schroder, J. C., Campuzano-Jost, P., Day, D. A., Shah, V., Larson, K., Sommers, J. M., Sullivan, A. P., Campos, T., Reeves, J. M., Hills, A., Hornbrook, R. S., Blake, N. J., Scheuer, E., Guo, H., Fibiger, D. L., McDuffie, E. E., Hayes, P. L., Weber, R. J., Dibb, J. E., Apel, E. C., Jaegle, L., Brown, S. S., Thornton, J. A., and Jimenez, J. L.: Sources and Secondary Production of Organic Aerosols in the Northeastern United States during WINTER, J. Geophys. Res. Atmos., 123, 7771-7796, https://doi.org/10.1029/2018JD028475, 2018.

Sharma, G., Sinha, B., Pallavi, Hakkim, H., Chandra, B. P., Kumar, A., and Sinha, V.: Gridded Emissions of CO, NO_x, SO_2, CO_2, NH_3, HCl, CH_4, $PM_{2.5}$, PM_{10}, BC, and NMVOC from Open Municipal Waste Burning in India, Environ. Sci. Technol., 53, 4765-4774, https://doi.org/10.1021/acs.est.8b07076, 2019.

Shen, G., Xiong, R., Tian, Y., Luo, Z., Jiangtulu, B., Meng, W., Du, W., Meng, J., Chen, Y., Xue, B., Wang, B., Duan, Y., Duo, J., Fan, F., Huang, L., Ju, T., Liu, F., Li, S., Liu, X., Li, Y., Wang, M., Nan, Y., Pan, B., Pan, Y., Wang, L., Zeng, E., Zhan, C., Chen, Y., Shen, H., Cheng, H., and Tao, S.: Substantial transition to clean household energy mix in rural China, Natl. Sci. Rev., 9, https://doi.org/10.1093/nsr/nwac050, 2022.

Shiraiwa, M., Ueda, K., Pozzer, A., Lammel, G., Kampf, C. J., Fushimi, A., Enami, S., Arangio, A. M., Frohlich-Nowoisky, J., Fujitani, Y., Furuyama, A., Lakey, P. S. J., Lelieveld, J., Lucas, K., Morino, Y., Poschl, U., Takahama, S., Takami, A., Tong, H., Weber, B., Yoshino, A., and Sato, K.: Aerosol Health Effects from Molecular to Global Scales, Environ. Sci. Technol., 51, 13545-13567, https://doi.org/10.1021/acs.est.7b04417, 2017.

Shrivastava, M., Easter, R. C., Liu, X. H., Zelenyuk, A., Singh, B., Zhang, K., Ma, P. L., Chand, D., Ghan, S., Jimenez, J. L., Zhang, Q., Fast, J., Rasch, P. J., and Tiitta, P.: Global transformation and fate of SOA: Implications of low-volatility SOA and gas-phase fragmentation reactions, J. Geophys. Res. Atmos., 120, 4169-4195, https://doi.org/10.1002/2014JD022563, 2015.

Shrivastava, M., Cappa, C. D., Fan, J. W., Goldstein, A. H., Guenther, A. B., Jimenez, J. L., Kuang, C., Laskin, A., Martin, S. T., Ng, N. L., Petaja, T., Pierce, J. R., Rasch, P. J., Roldin, P., Seinfeld, J. H., Shilling, J., Smith, J. N., Thornton, J. A., Volkamer, R., Wang, J., Worsnop, D. R., Zaveri, R. A., Zelenyuk, A., and Zhang, Q.: Recent advances in understanding secondary organic aerosol: Implications for global climate forcing, Rev. Geophys., 55, 509-559, https://doi.org/10.1002/2016RG000540, 2017.

Shrivastava, M. K., Lipsky, E. M., Stanier, C. O., and Robinson, A. L.: Modeling Semivolatile Organic Aerosol Mass Emissions from Combustion Systems, Environ. Sci. Technol., 40, 2671-2677, https://doi.org/10.1021/es0522231, 2006.

Shrivastava, M. K., Lane, T. E., Donahue, N. M., Pandis, S. N., and Robinson, A. L.: Effects of gas particle partitioning and aging of primary emissions on urban and regional organic aerosol concentrations, J. Geophys. Res. Atmos., 113, https://doi.org/10.1029/2007jd009735, 2008.

Spracklen, D. V., Jimenez, J. L., Carslaw, K. S., Worsnop, D. R., Evans, M. J., Mann, G. W., Zhang, Q., Canagaratna, M. R., Allan, J., Coe, H., McFiggans, G., Rap, A., and Forster, P.: Aerosol mass spectrometer constraint on the global secondary organic aerosol budget, Atmos. Chem. Phys., 11, 12109-12136, https://doi.org/10.5194/acp-11-12109-2011, 2011.

Thalman, R., de Sá, S. S., Palm, B. B., Barbosa, H. M. J., Pöhlker, M. L., Alexander, M. L., Brito, J., Carbone, S., Castillo, P., Day, D. A., Kuang, C., Manzi, A., Ng, N. L., Sedlacek Iii, A. J., Souza, R., Springston, S., Watson, T., Pöhlker, C., Pöschl, U., Andreae, M. O., Artaxo, P., Jimenez, J. L., Martin, S. T., and Wang, J.: CCN activity and organic hygroscopicity of aerosols downwind of an urban region in central Amazonia: seasonal and diel variations and impact of anthropogenic emissions, Atmos. Chem. Phys., 17, 11779-11801, https://doi.org/10.5194/acp-17-11779-2017, 2017.

Tilmes, S., Hodzic, A., Emmons, L. K., Mills, M. J., Gettelman, A., Kinnison, D. E., Park, M., Lamarque, J. F., Vitt, F., Shrivastava, M., Campuzano-Jost, P., Jimenez, J. L., and Liu, X.: Climate Forcing and Trends of Organic Aerosols in the Community Earth System Model (CESM2), J. Adv. Model. Earth Syst., n/a, https://doi.org/10.1029/2019ms001827, 2019.

https://doi.org/10.5194/egusphere-2026-3160
Preprint. Discussion started: 23 June 2026

Tkacik, D. S., Presto, A. A., Donahue, N. M., and Robinson, A. L.: Secondary Organic Aerosol Formation from Intermediate-Volatility Organic Compounds: Cyclic, Linear, and Branched Alkanes, Environ. Sci. Technol., 46, 8773-8781, https://doi.org/10.1021/es301112c, 2012.

Tsigaridis, K., Daskalakis, N., Kanakidou, M., Adams, P. J., Artaxo, P., Bahadur, R., Balkanski, Y., Bauer, S. E., Bellouin, N., Benedetti, A., Bergman, T., Berntsen, T. K., Beukes, J. P., Bian, H., Carslaw, K. S., Chin, M., Curci, G., Diehl, T., Easter, R. C., Ghan, S. J., Gong, S. L., Hodzic, A., Hoyle, C. R., Iversen, T., Jathar, S., Jimenez, J. L., Kaiser, J. W., Kirkevåg, A., Koch, D., Kokkola, H., Lee, Y. H., Lin, G., Liu, X., Luo, G., Ma, X., Mann, G. W., Mihalopoulos, N., Morcrette, J. J., Müller, J. F., Myhre, G., Myriokefalitakis, S., Ng, N. L., O'Donnell, D., Penner, J. E., Pozzoli, L., Pringle, K. J., Russell, L. M., Schulz, M., Sciare, J., Seland, Ø., Shindell, D. T., Sillman, S., Skeie, R. B., Spracklen, D., Stavrakou, T., Steenrod, S. D., Takemura, T., Tiitta, P., Tilmes, S., Tost, H., van Noije, T., van Zyl, P. G., von Salzen, K., Yu, F., Wang, Z., Wang, Z., Zaveri, R. A., Zhang, H., Zhang, K., Zhang, Q., and Zhang, X.: The AeroCom evaluation and intercomparison of organic aerosol in global models, Atmos. Chem. Phys., 14, 10845-10895, https://doi.org/10.5194/acp-14-10845-2014, 2014.

Tsimpidi, A. P., Karydis, V. A., Pandis, S. N., and Lelieveld, J.: Global combustion sources of organic aerosols: model comparison with 84 AMS factor-analysis data sets, Atmos. Chem. Phys., 16, 8939-8962, https://doi.org/10.5194/acp-16-8939-2016, 2016.

Tsimpidi, A. P., Karydis, V. A., Pandis, S. N., and Lelieveld, J.: Global-scale combustion sources of organic aerosols: sensitivity to formation and removal mechanisms, Atmos. Chem. Phys., 17, 7345-7364, https://doi.org/10.5194/acp-17-7345-2017, 2017.

Tsimpidi, A. P., Scholz, S. M. C., Milousis, A., Mihalopoulos, N., and Karydis, V. A.: Aerosol composition trends during 2000–2020: in-depth insights from model predictions and multiple worldwide near-surface observation datasets, Atmos. Chem. Phys., 25, 10183-10213, https://doi.org/10.5194/acp-25-10183-2025, 2025.

Verma, V., Fang, T., Xu, L., Peltier, R. E., Russell, A. G., Ng, N. L., and Weber, R. J.: Organic Aerosols Associated with the Generation of Reactive Oxygen Species (ROS) by Water-Soluble PM2.5, Environ. Sci. Technol., 49, 4646-4656, https://doi.org/10.1021/es505577w, 2015.

Wang, X., Chakrabarty, R. K., Schwarz, J. P., Murphy, S. M., Levin, E. J. T., Howell, S. G., Guo, H., Campuzano-Jost, P., and Jimenez, J. L.: Dark brown carbon from biomass burning contributes to significant global-scale positive forcing, One Earth, 8, https://doi.org/10.1016/j.oneear.2025.101205, 2025.

Wang, Y., Jacob, D. J., and Logan, J. A.: Global simulation of tropospheric O_3-NO_x-hydrocarbon chemistry: 1. Model formulation, J. Geophys. Res. Atmos., 103, 10713-10725, https://doi.org/10.1029/98jd00158, 1998.

Wiedinmyer, C., Kimura, Y., McDonald-Buller, E. C., Emmons, L. K., Buchholz, R. R., Tang, W., Seto, K., Joseph, M. B., Barsanti, K. C., Carlton, A. G., and Yokelson, R.: The Fire Inventory from NCAR version 2.5: an updated global fire emissions model for climate and chemistry applications, Geosci. Model Dev., 16, 3873-3891, https://doi.org/10.5194/gmd-16-3873-2023, 2023.

Woody, M. C., Baker, K. R., Hayes, P. L., Jimenez, J. L., Koo, B., and Pye, H. O. T.: Understanding sources of organic aerosol during CalNex-2010 using the CMAQ-VBS, Atmos. Chem. Phys., 16, 4081-4100, https://doi.org/10.5194/acp-16-4081-2016, 2016.

Wu, W., Fu, T.-M., Arnold, S. R., Spracklen, D. V., Zhang, A., Tao, W., Wang, X., Hou, Y., Mo, J., Chen, J., Li, Y., Feng, X., Lin, H., Huang, Z., Zheng, J., Shen, H., Zhu, L., Wang, C., Ye, J., and Yang, X.: Temperature-Dependent Evaporative Anthropogenic VOC Emissions Significantly Exacerbate Regional Ozone Pollution, Environ. Sci. Technol., https://doi.org/10.1021/acs.est.3c09122, 2024.

Xu, R., Miao, R., Li, J., Ma, H., Hu, H., Wang, H., Yan, X., Liu, X., Tong, D., Geng, G., Chen, Q., He, K., and Zhang, Q.: Global emission trends of anthropogenic full-volatility-range organic compounds 1970-2020, Natl. Sci. Rev., https://doi.org/10.1093/nsr/nwag281, 2026.

https://doi.org/10.5194/egusphere-2026-3160
Preprint. Discussion started: 23 June 2026

Yang, N., Wang, Q., Xiong, Q., Fan, Z., Liu, G., Li, F., Zhu, S., Zhou, Y., Tao, J., Hong, J., Wang, H., Huang, C., Sun, Y., Cheng, Y., Su, H., and Ma, N.: Intermediate-Volatility Organic Compounds (IVOCs) Emissions Based on Source-Specific Emission Ratios Relative to NonMethane Volatile Organic Compounds (NMVOCs) Give Better Representation of the Spatial Distribution of IVOCs in China, J. Geophys. Res. Atmos., 130, e2024JD041464, https://doi.org/10.1029/2024JD041464, 2025.

Zhang, L. M., Gong, S. L., Padro, J., and Barrie, L.: A size-segregated particle dry deposition scheme for an atmospheric aerosol module, Atmos. Environ., 35, 549-560, https://doi.org/10.1016/S1352-2310(00)00326-5, 2001.

Zhang, X., Cappa, C. D., Jathar, S. H., McVay, R. C., Ensberg, J. J., Kleeman, M. J., and Seinfeld, J. H.: Influence of vapor wall loss in laboratory chambers on yields of secondary organic aerosol, Proc. Natl. Acad. Sci. U. S. A., 111, 5802-5807, https://doi.org/10.1073/pnas.1404727111, 2014.

Zhao, Y., Hennigan, C. J., May, A. A., Tkacik, D. S., de Gouw, J. A., Gilman, J. B., Kuster, W. C., Borbon, A., and Robinson, A. L.: Intermediate-volatility organic compounds: a large source of secondary organic aerosol, Environ. Sci. Technol., 48, 13743-13750, https://doi.org/10.1021/es5035188, 2014.

Zheng, Y., Chen, Q., Cheng, X., Mohr, C., Cai, J., Huang, W., Shrivastava, M., Ye, P., Fu, P., Shi, X., Ge, Y., Liao, K., Miao, R., Qiu, X., Koenig, T. K., and Chen, S.: Precursors and Pathways Leading to Enhanced Secondary Organic Aerosol Formation during Severe Haze Episodes, Environ. Sci. Technol., 55, 15680-15693, https://doi.org/10.1021/acs.est.1c04255, 2021.

Zheng, Y., Miao, R., Zhang, Q., Li, Y., Cheng, X., Liao, K., Koenig, T. K., Ge, Y., Tang, L., Shang, D., Hu, M., Chen, S., and Chen, Q.: Secondary Formation of Submicron and Supermicron Organic and Inorganic Aerosols in a Highly Polluted Urban Area, J. Geophys. Res. Atmos., 128, e2022JD037865, https://doi.org/10.1029/2022JD037865, 2023.

https://doi.org/10.5194/egusphere-2026-3160
Preprint. Discussion started: 23 June 2026

775

780

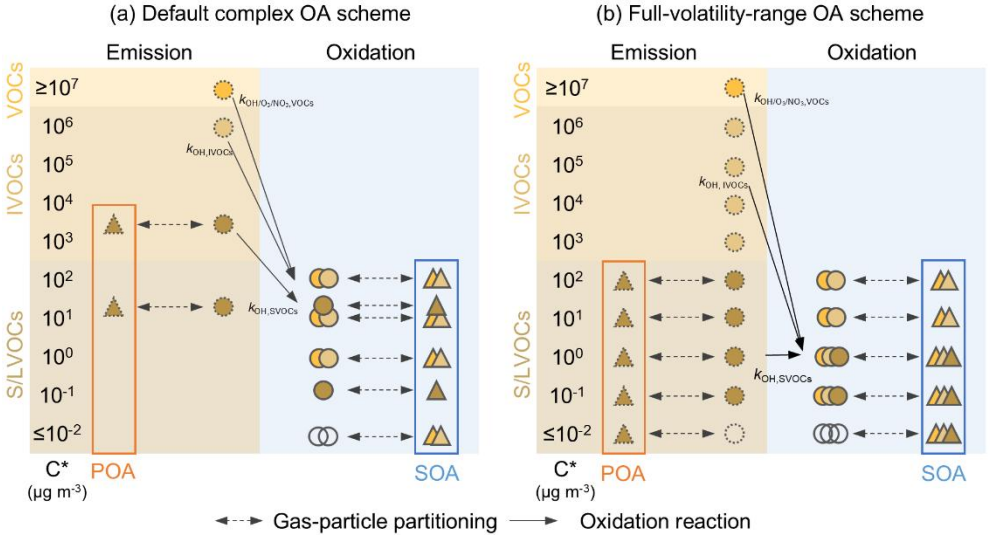

Figure 1. Schematic diagram of the POA and SOA formation from VOC, IVOC, and S/LVOC precursors in the (a) default complex OA and (b) full-volatility-range OA schemes. Colored circles and triangles represent model tracers of gaseous precursors, 785 **oxidation products, and OA components. For C* ≤10^{-2} ug m^{-3}, OA components mostly remain the particle phase at ambient conditions and thus their gaseous tracers (open circles) are ignored in the model scheme.**

https://doi.org/10.5194/egusphere-2026-3160
Preprint. Discussion started: 23 June 2026

790

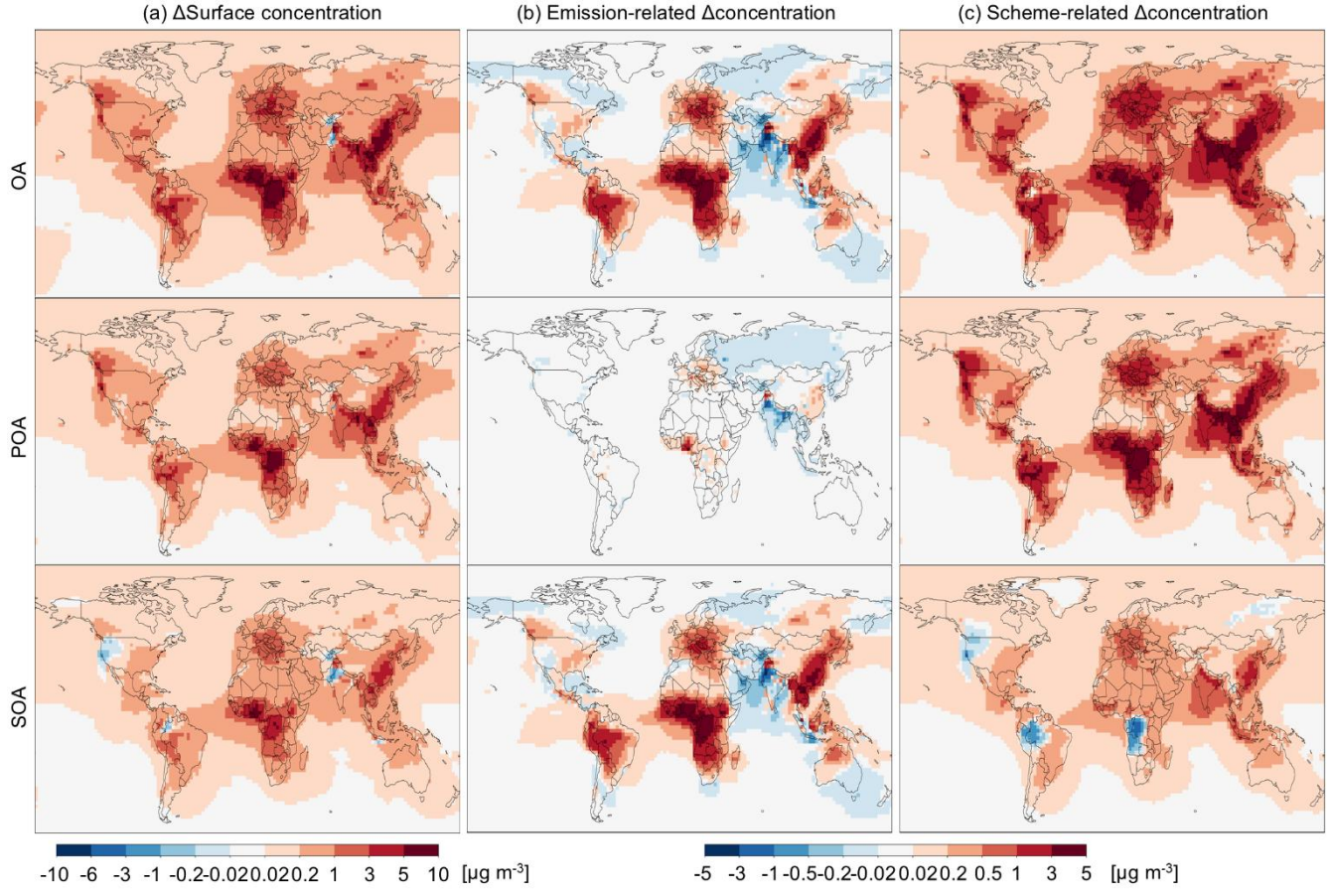

795 **Figure 2. The differences of annual-mean surface concentrations of OA, POA, and SOA between different simulation runs in GEOS-Chem (Table S4), including (a) the overall changes calculated as "Base" – "Default", (b) the emission-related changes calculated as "Default_emis" – "Default", and (c) the scheme-related changes calculated as "Base" – "Default_emis".**

https://doi.org/10.5194/egusphere-2026-3160
Preprint. Discussion started: 23 June 2026

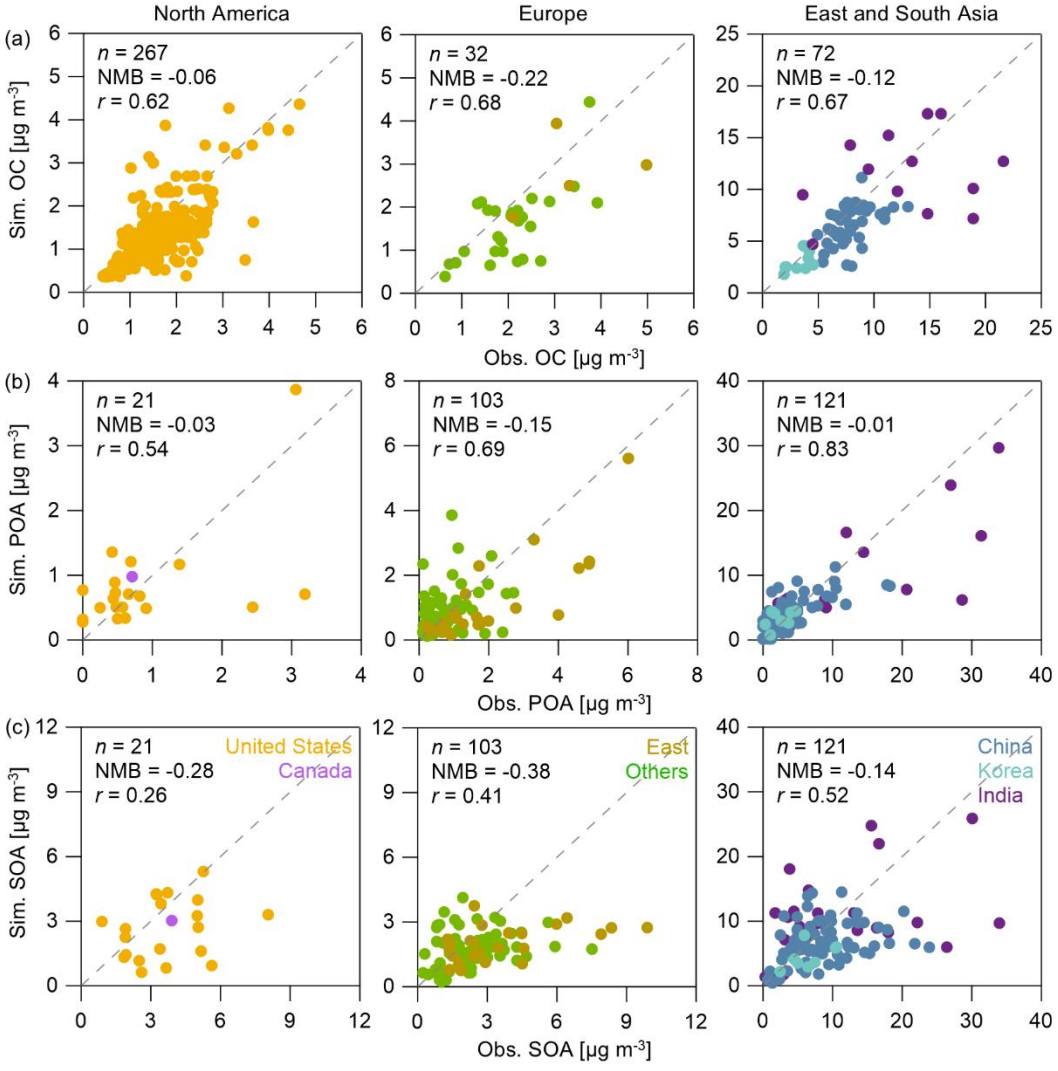

Figure 3. Scatter plots of the observed and simulated ("Base") concentrations of (a) OC, (b) POA, and (c) SOA in North America, Europe, and East and South Asia. East European countries include Poland, Romania, Estonia, Lithuania, Greece, and Cyprus. Other European countries include Czech, Germany, Switzerland, Finland, Norway, Spain, Italy, France, Ireland, Netherland, and United Kingdom. The OC data are annual mean surface concentrations taken from various monitoring networks. The POA and SOA data are the campaign-mean concentrations derived from the source-apportionment results of the surface AMS or ACSM measurements.

https://doi.org/10.5194/egusphere-2026-3160
Preprint. Discussion started: 23 June 2026

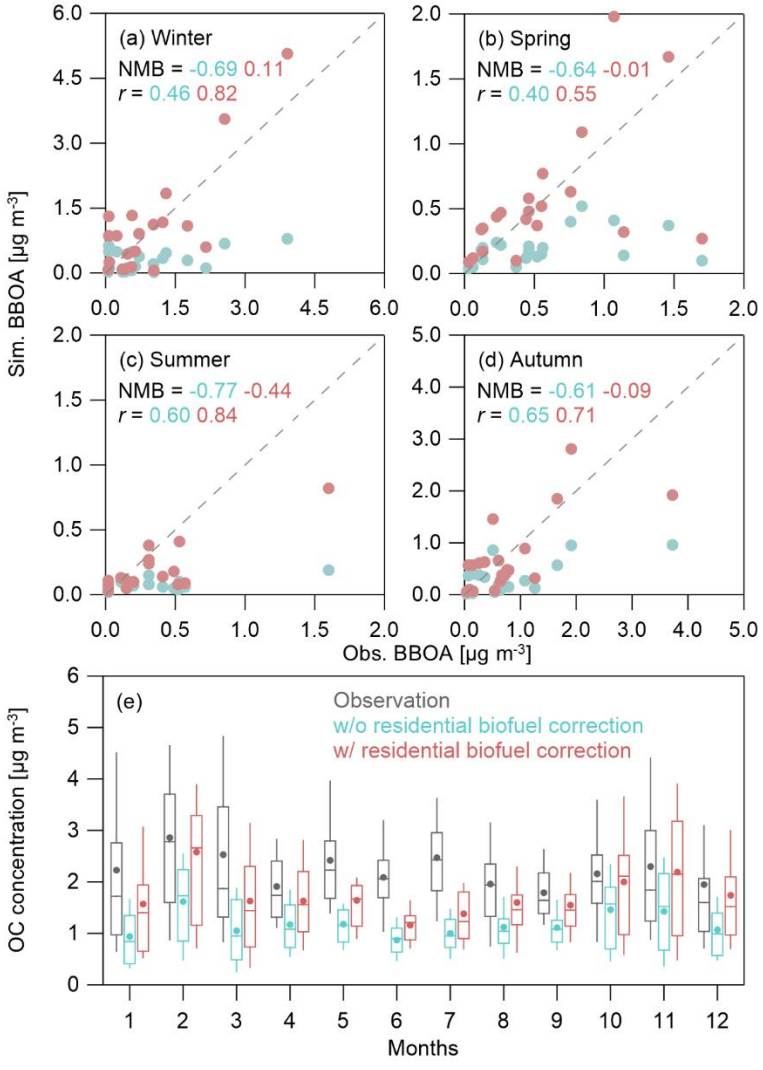

Figure 4. (a-d) Scatter plots of the observation-derived and simulated ("Base") concentrations of BBOA in Europe in the four seasons. (e) The box-and-whisker plots of the observed and simulated monthly OC concentrations in Europe. The upper and lower edges of the boxes, the whiskers, the middle lines, and the solid dots denote the 25th and 75th percentiles, the 10th and 90th percentiles, the median values, and the mean values of OC concentrations, respectively.

https://doi.org/10.5194/egusphere-2026-3160
Preprint. Discussion started: 23 June 2026

825

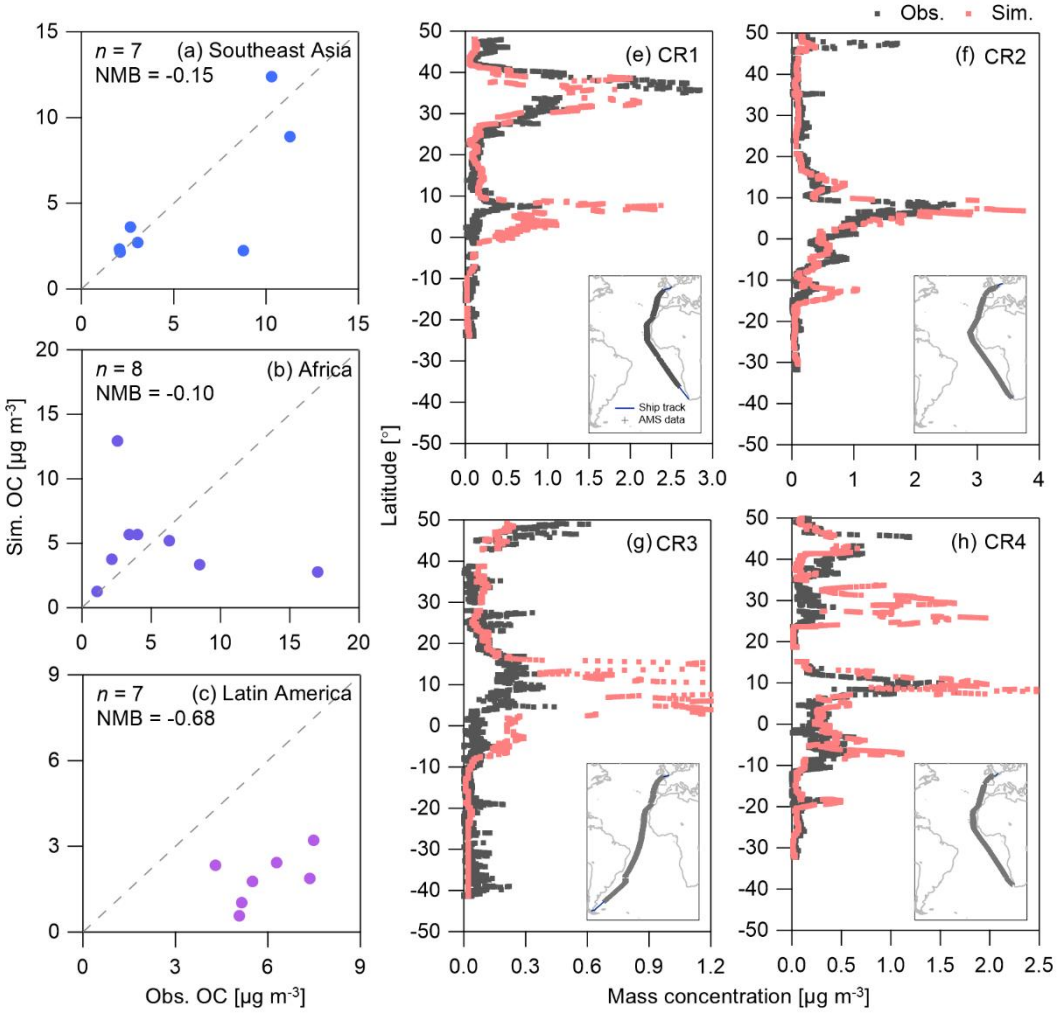

Figure 5. (a-c) Scatter plots of the observed and simulated ("Base") mass concentrations of OC in Southeast Asia, Africa, and Latin America. (e-h) Comparisons of the observation-derived and simulated latitudinal profile of non-marine SOA from four shipborne campaigns, CR1 to CR4, in the Atlantic Ocean.

830

https://doi.org/10.5194/egusphere-2026-3160
Preprint. Discussion started: 23 June 2026

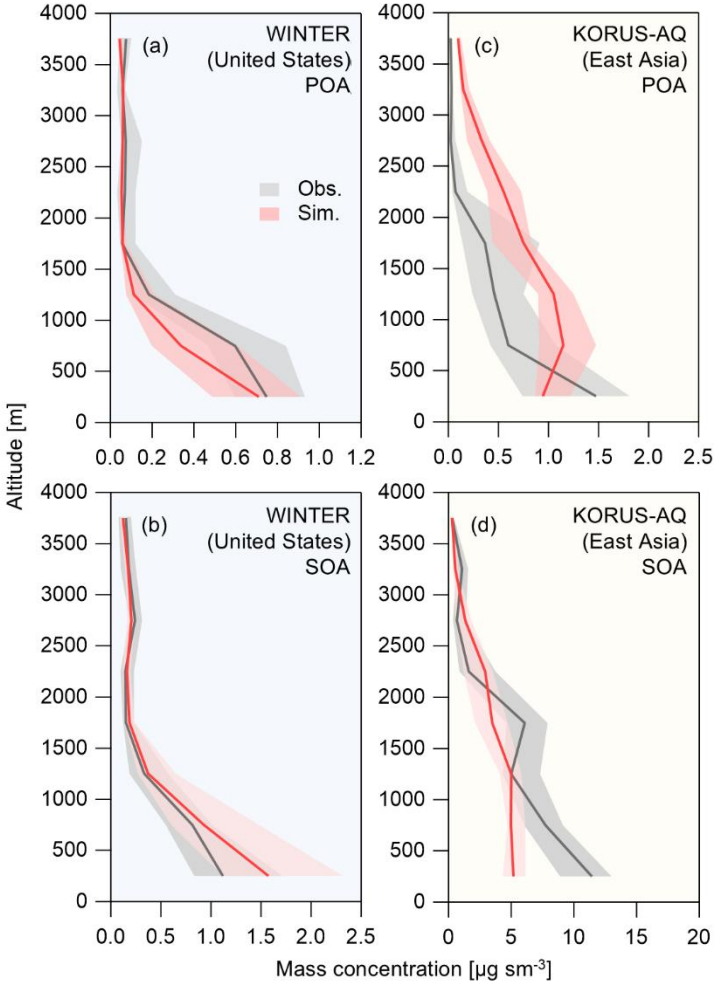

Figure 6. Comparisons of the observation-derived and simulated ("Base") vertical profiles of POA and SOA concentrations for the WINTER and KORUS-AQ aircraft campaigns.

https://doi.org/10.5194/egusphere-2026-3160
Preprint. Discussion started: 23 June 2026

845

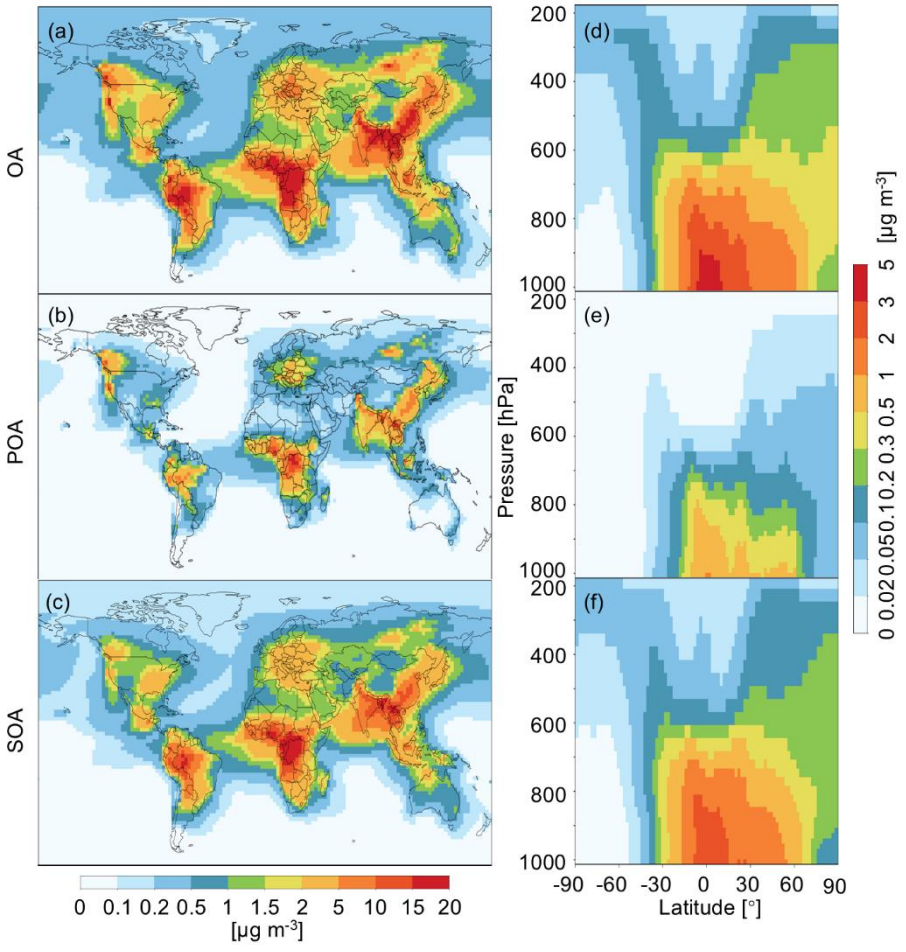

Figure 7. Simulated annual-mean (a-c) surface and (d-f) zonal mean concentrations of OA, POA, and SOA in the year of 2018 from the full-volatility-range OA runs ("Base").

850

https://doi.org/10.5194/egusphere-2026-3160
Preprint. Discussion started: 23 June 2026

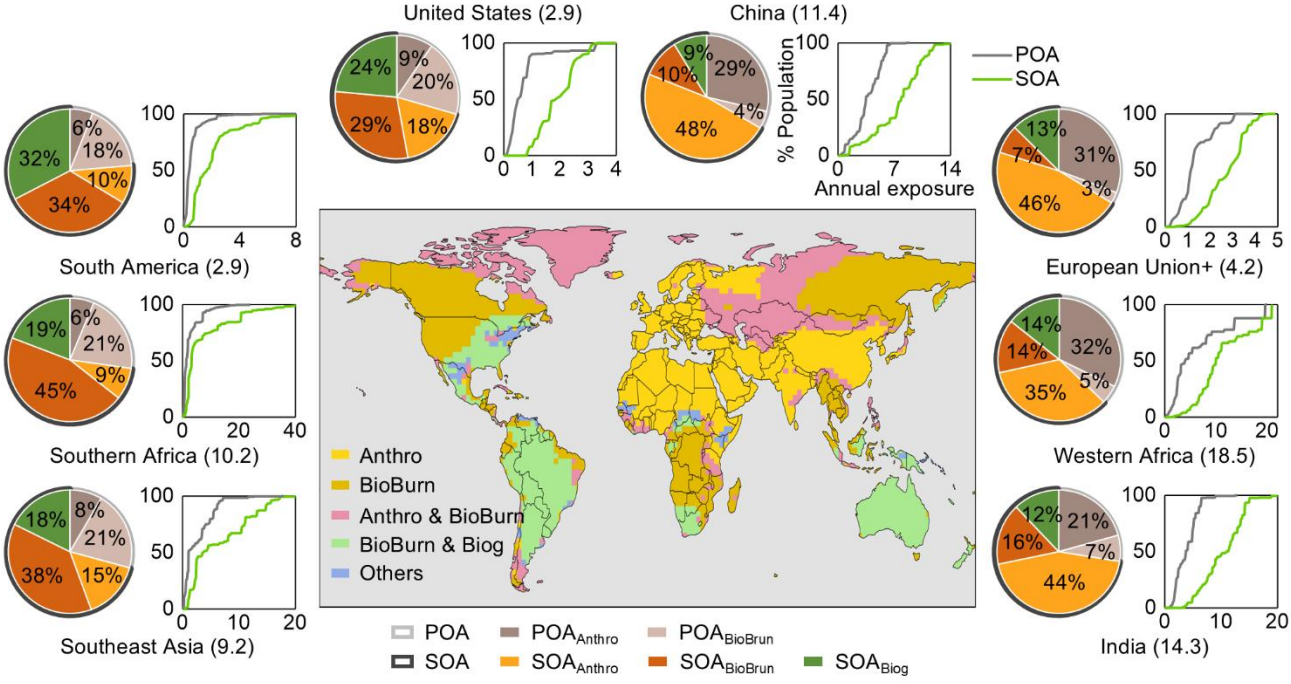

Figure 8. Sources that contribute to over 30% of annual-mean surface OA concentrations in 2018. Pie charts illustrate the mass fractions of different types of POA and SOA in population-weighted OA concentrations, and cumulative distributions represent the population percentages exposed to POA and SOA concentrations (in the unit of μg m^{-3}) in different regions and countries. The numbers in parentheses indicate population-weighted OA concentrations. "Anthro", "BioBurn", and "Biog" represent anthropogenic, open biomass burning, and biogenic sources, respectively. European Union+ encompasses the 27 member states of European Union, along with Norway, Switzerland, and Liechtenstein. Southern America includes Argentina, Bolivia, Brazil, Chile, Colombia, Ecuador, Guyana, Paraguay, Peru, Suriname, Uruguay, and Venezuela. Western Africa includes Benin, Burkina Faso, Cape Verde, The Gambia, Ghana, Guinea, Guinea-Bissau, Ivory Coast, Liberia, Mali, Mauritania, Niger, Nigeria, Senegal, Sierra Leone, and Togo. Southern Africa includes Angola, Botswana, Comoros, Congo, Eswatini, Lesotho, Madagascar, Malawi, Mauritius, Mozambique, Namibia, Seychelles, South Africa, Tanzania, Zambia, and Zimbabwe.

https://doi.org/10.5194/egusphere-2026-3160
Preprint. Discussion started: 23 June 2026

875

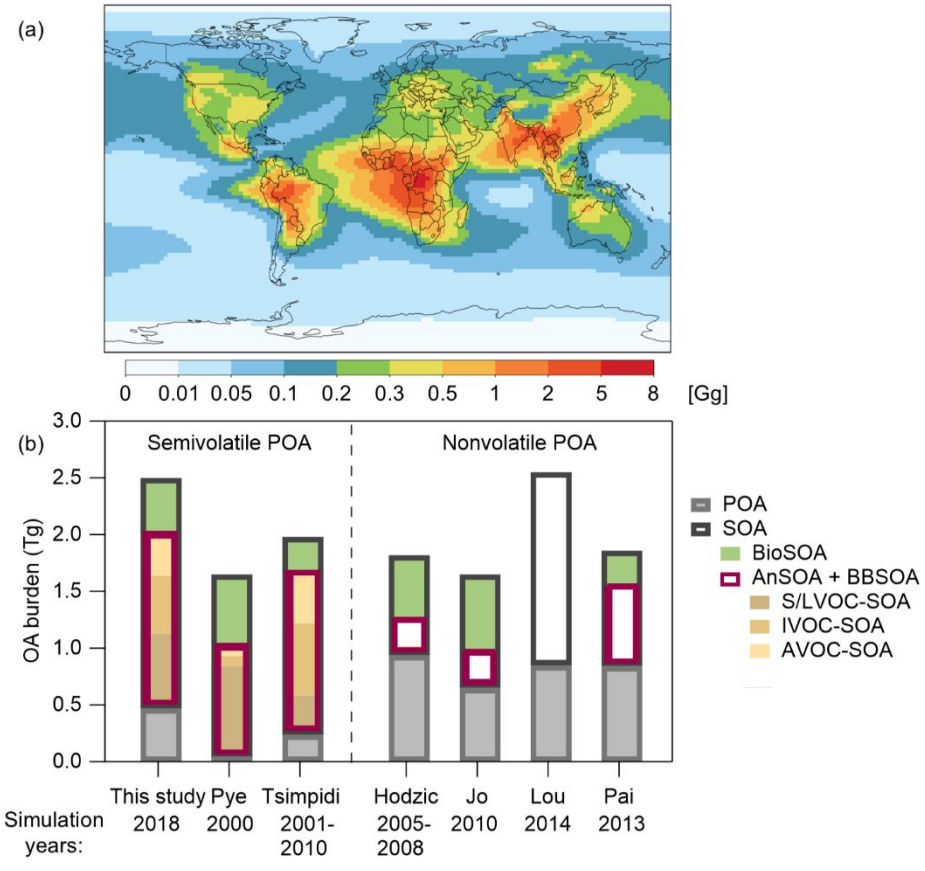

880 **Figure 9. (a) Simulated global OA burden in 2018 ("Base"). (b) Comparisons of global OA burden estimates, including the "Revised Simulation" from Pye and Seinfeld (2010), "NY_DPH run" from Hodzic et al. (2016), "CAM-Chem simulation" from Jo et al. (2023), "FRAG50_PHO" from Lou et al. (2020), and "Simple scheme" Pai et al. (2020). The simulation years for all the studies are shown.**

https://doi.org/10.5194/egusphere-2026-3160
Preprint. Discussion started: 23 June 2026

885

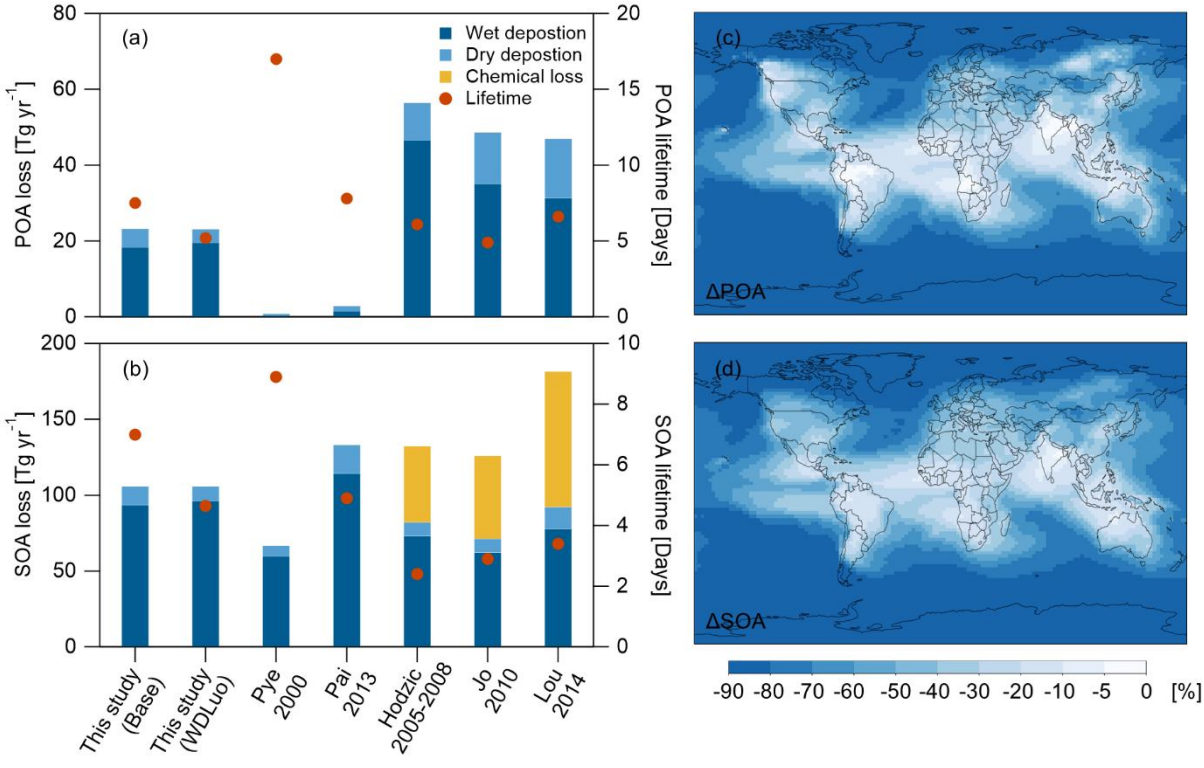

890

Figure 10. (a-b) Comparisons of the estimated global loss and global mean lifetime of POA and SOA among studies. (c-d) The differences in POA and SOA burdens between the simulations with default wet deposition parameterization and the parameterization from Luo et al. (2020) ("WDLuo"– "Base").

895

https://doi.org/10.5194/egusphere-2026-3160
Preprint. Discussion started: 23 June 2026

Table 1. Global budgets for OA and its components for the year 2018 ("Base").

	Net production (Tg yr^{-1})	Dry deposition (Tg yr^{-1})	Wet deposition (Tg yr^{-1})	Burden (Tg)	Lifetime (days)
POA	**23.0**	**4.8**	**18.3**	**0.5**	**7.5**
SOA	**105.6**	**12.3**	**93.3**	**2.0**	**7.0**
S/LVOC-SOA	21.0	3.6	17.4	0.7	11.5
IVOC-SOA	31.8	3.2	28.6	0.5	5.8
AVOC-SOA*	19.4	1.9	17.5	0.4	7.2
Terpene-SOA	12.4	1.6	10.8	0.2	4.5
Isoprene-SOA*	21.0	2.0	19.1	0.3	5.7
OA	**128.6**	**17.1**	**111.5**	**2.5**	**7.1**
Anthropogenic OA	27.6	3.7	23.8	0.7	8.6
Biogenic OA	37.0	3.6	33.4	0.5	5.3
Open biomass burning OA	64.1	9.8	54.3	1.3	7.5

*: included the SOA formed from glyoxal and methylglyoxal.